OPTIMAL DESIGN OF NONLINEAR ENERGY SINKS FOR SDOF STRUCTURES SUBJECTED TO WHITE NOISE BASE EXCITATIONS

Maria Oliva[1], Giorgio Barone[2] and Giacomo Navarra[1]

[1]Faculty of Engineering and Architecture, University of Enna Kore, Cittadella Universitaria, Enna, Italy
[2]School of Civil and Building Engineering, Loughborough University, Loughborough, Leicestershire, UK

Abstract

Nonlinear Energy Sinks (NESs) have recently received increasing attention from researchers because of their capability to passively absorb a significant amount of energy over a wide range of frequencies. In most studies, the dynamic response of the main structure coupled with one or more NESs is analysed for impulsive loading. In this paper, the performance of the NES attached to a Single Degree of Freedom (SDOF) system, under random Gaussian white noise base excitations, is investigated through several numerical simulations. In order to determine the optimal configuration for the device, four different objective functions are considered. Sensitivity analyses with respect to the intensity of the random loads, the mass ratio and the main parameters of the primary structure are presented. The authors propose an approximate design approach based on the use of the Statistical Linearization Technique, and an accurate empirical formulation linking the NES optimal parameters to the characteristic of the main structure and the random excitation. Numerical results are validated by Monte Carlo simulations. Finally, a numerical application for a 2-DOFs system equipped with a NES has been presented in order to investigate the applicability of the proposed empirical approach for Multi Degrees of Freedom structures.

Author keywords: Nonlinear Energy Sink; Passive Control; Optimisation; Structural dynamics; White Noise; Statistical Linearization Technique.

1. INTRODUCTION

The growing urbanization and the constant advances in building technologies have led to increasingly tall, slender and lightweight structures, often vulnerable to dynamic loads (e.g. wind and earthquakes). In the last decades several control strategies [1] have been developed to protect tall structures against environmental actions, thus reducing structural vibrations. Dynamic vibration absorbers belong to the class of passive control systems. These devices have been widely used for civil engineering structures because of their capability to operate without requiring an external power source. This implies simplicity in design, maintenance and operation. However, conventional linear dynamic vibration absorbers are generally tuned to one of the modal frequencies of the main structure in order to suppress the contributions from fundamental modes. Consequently, they are very sensitive to the detuning, caused for example by creep, temperature effects or significant variation of the structural parameters.

The Nonlinear Energy Sink (NES) is able to resonate with any mode of the primary structure because of its nonlinear nature. It is, therefore, insensitive to frequency changes and more robust than linear Tuned Mass Dampers (TMDs) [2]. The NES consists of a small mass coupled to the main structure with a nonlinear spring and a damping element. It is capable to passively and irreversibly absorb and dissipate a significant amount of energy from the primary structure over a wide range of frequencies. This one-way irreversible transfer, known as passive target energy transfer, occurs in systems of damped oscillators mainly via transient resonance capture and has been widely investigated both analytically [3–8] and experimentally [9–14]. NES configurations can be categorized depending on the operating mechanisms, as grounded [3,4] or ungrounded [5,6], and as smooth [7,15,16] or non-smooth [9,10]. Specifically, a grounded configuration consists of an essentially nonlinear grounded oscillator coupled to the primary structure through a weakly linear stiffness, whereas in an ungrounded one the NES is directly and strongly coupled to the primary structure through the essentially nonlinear stiffness; a smooth NES configuration involves a cubic nonlinear stiffness, whereas a non-smooth one involves nonlinearities in the form of clearances or vibro-impacts. The performance of these types of NES has been numerically studied and experimentally tested under different loading conditions, such as impulsive [6,14,16,17], periodic [18–21], seismic [10,13,14,22] and stationary random loadings [2].

Despite the high capacity of this nonlinear absorber to reduce the dynamic response of the structures, the presence of the nonlinear stiffness term makes the NESs especially sensitive to loading perturbations. Therefore, the optimal design of the device parameters is of the utmost importance. Several optimisation criteria and objective functions have been introduced in literature, depending on the characteristics of the main system and the external excitations. In [23,24], a procedure to obtain optimal design of the energetic sinks with amplitude-phase variables has been proposed by considering the analytical solution of energy pumping problem for strongly nonhomogeneous two-Degree of Freedom (DOF) systems. A closed-form solution for the nonlinear stiffness of the NES bounds of stability has been proposed in reference [25], whereas an analytical tuning for the nonlinear stiffness of the NES under transient and harmonic excitations has been proposed in [26]. In [27], optimal design criteria to determine the minimum nonlinear stiffness required to activate the target energy transfer have been proposed for transient regime. A reliability-based design optimisation of the NES has been presented in reference [28] for the cases of two- and three- DOFs systems, under impulsive loading. Genetic Algorithms have been used to find the optimal parameters of NESs in order to mitigate the vibrations of beams subjected to moving loads in [29].

44　The performance of a NES coupled to a linear damped Eulero-Bernoulli beam has been also
45　considered in [30], where an optimisation procedure has been performed for various boundary
46　conditions with two different values of forcing amplitude. A two-DOFs structure, subjected to a band-
47　limited white noise, has been investigated in [2]. In the latter study, the authors have shown that the
48　optimal nonlinear stiffness decreases for increasing amplitude of the load. Moreover, the performance
49　of the NES increases with the natural frequency of the main structure. However, these results have
50　been obtained considering only one sample of white noise.
51　　　In this paper, the optimal parameters of a smooth ungrounded NES have been investigated for the
52　case of a structure subjected to random base excitations, modelled as samples of a random Gaussian
53　white noise process. The aim of this work is to analyse the dependence of the optimal NES parameters
54　on the main structure characteristics and on the intensity of the random excitation in order to define a
55　simplified optimisation procedure.
56　　　First, a simplified approach based on the Statistical Linearization Technique (SLT) has been used
57　to obtain an approximate formula for the optimal nonlinear stiffness of the NES. The formula has been
58　determined minimising the mean square error between the nonlinear system and the linearised one,
59　subjected both to the same Gaussian excitation. The results have been compared with Monte Carlo
60　simulations, in order to determine the error committed in evaluating the optimal parameters.
61　　　Then, a parametric analysis has been performed in order to investigate the dependence of the NES
62　performance on the main characteristics of the system by varying the intensity of the random loading,
63　the mass ratio between the NES and the primary structure, as well as the frequency and the damping
64　ratio of the main structure. The numerical results are critically discussed, focusing on the sensitivity of
65　the NES optimal nonlinear stiffness and linear damping. Empirical relationships among the optimal
66　parameters, the amplitude of the load and the main system parameters are proposed for pre-design
67　purposes and validated against the results of Monte Carlo simulations. Moreover, a simplified design
68　of NESs for MDOF systems which involves the application of these empirical formulae is presented
69　through a numerical application on a 2DOF model.

70

2. STRUCTURAL MODEL

72　A schematic diagram of the system considered herein is shown in Figure 1. Known in literature as
73　"Configuration II" [8] or "Type I" [22,31] NES, it consists of a SDOF primary structure connected to
74　an ungrounded and lightweight NES through a pure cubic stiffness and a linear viscous damper. The
75　equations of motion of the combined system can be written as following:

76
$$\begin{cases} m_1\ddot{x}_1 + c_1\dot{x}_1 + c_2\left(\dot{x}_1 - \dot{x}_2\right) + k_1 x_1 + k_2\left(x_1 - x_2\right)^3 = -m_1\ddot{x}_g \\ m_2\ddot{x}_2 + c_2\left(\dot{x}_2 - \dot{x}_1\right) + k_2\left(x_2 - x_1\right)^3 = -m_2\ddot{x}_g \end{cases} \tag{1}$$

77　in which m_1, c_1, k_1 and x_1 are mass, viscous damping coefficient, stiffness coefficient and
78　displacement relative to the base of the main structure, respectively; m_2, c_2, k_2 and x_2 are mass,
79　viscous damping coefficient, nonlinear stiffness coefficient and displacement relative to the base of the
80　NES, respectively; dots mean derivative with respect to time, and $\ddot{x}_g$ is the base acceleration modelled
81　as a zero-mean stationary Gaussian white noise, having Power Spectral Density (PSD) amplitude S_0.
82　　　Dividing Eq. (1) by m_1, the nonlinear system of equations becomes:

83
$$\begin{cases} \ddot{x}_1 + \lambda_1 \dot{x}_1 + \lambda_2 \left(\dot{x}_1 - \dot{x}_2 \right) + \omega_1^2 x_1 + \kappa \left(x_1 - x_2 \right)^3 = -\ddot{x}_g \\ \varepsilon \ddot{x}_2 + \lambda_2 \left(\dot{x}_2 - \dot{x}_1 \right) + \kappa \left(x_2 - x_1 \right)^3 = -\varepsilon \ddot{x}_g \end{cases}$$
(2)

84   in which:

85
$$\lambda_1 = \frac{c_1}{m_1} = 2\zeta_1\omega_1; \quad \lambda_2 = \frac{c_2}{m_1}; \quad \omega_1^2 = \frac{k_1}{m_1}; \quad \kappa = \frac{k_2}{m_1}; \quad \varepsilon = \frac{m_2}{m_1}.$$

86   where ζ_1 and ω_1 are the damping ratio and the frequency of the primary structure and ε is the mass
87   ratio between the NES and the main structure. Several papers showed that even simple systems may
88   exhibit complex dynamics involving fundamental and sub-harmonic resonances, nonlinear beating
89   phenomena and multi-frequency responses [5,6,8].
90   An interesting feature of the NES is its ability to passively and irreversibly absorb and locally
91   dissipate a significant amount of vibrational energy from the primary structures. Moreover, the NES is
92   capable to interact over broad frequency bands, thus its performance is not significantly affected by
93   structural frequency changes and it is more robust than linear passive absorbers. However, the NES
94   performance is critically dependent on the amplitude of the external excitation since it was
95   demonstrated that it only works properly for specific ranges of forcing amplitudes. This is due to the
96   fact that the response of nonlinear systems is not proportional to the amplitude excitation, as it occurs
97   in linear ones. Therefore, the performance of a nonlinear system optimised for a specific load
98   condition can vary significantly for a different load.
99

100   **3. OPTIMAL NES PARAMETERS**

101   Although there are several papers discussing the NES and the nonlinear energy pumping phenomenon,
102   however only few of them aim to design optimal NES parameters for given primary system
103   specifications. This is due to the complex dynamic behaviour of the nonlinear system and the NES
104   sensitivity to loading perturbations that make particularly difficult designing the optimal parameters of
105   this device. Closed-form solutions to determine the optimal nonlinear stiffness of the NES capable to
106   trigger the targeted energy transfer have been proposed only for transient and harmonic excitations
107   [25–27], whereas, to the authors' knowledge, there are no analytical or numerical formulae for white
108   noise excitations.
109   Of course, the definition of the optimal NES parameters depends by the selected criteria used to
110   estimate the effectiveness of the NES itself. Herein, these criteria have been chosen among those
111   introduced in [32,33] and widely used to optimise different NES configurations [2,9,10,34]. Since in
112   this work the focus is on the protection of the main structure by reducing its response, the objective
113   functions have been defined as the dimensionless ratio between a selected characteristic of the
114   dynamic response of the primary structure in its controlled (i.e. with attached NES) and uncontrolled
115   (i.e. removing the NES) configurations, respectively. Therefore, these objective functions represent
116   different measures of the NES performance (the lower the value of each objective function, the higher
117   the NES performance) and their minimisation leads to determining the optimal NES parameters.
118   The first two objective functions consider the ratios of the Root Mean Square (RMS) of the
119   displacements and absolute accelerations of the controlled and uncontrolled systems, respectively, i.e.
120   they are defined as:

3

121
$$\hat{J}_1 = \frac{RMS(x_{1,C}(t))}{RMS(x_{1,U}(t))}$$
(3)

122
$$\hat{J}_2 = \frac{RMS(\ddot{x}_{1a,C}(t))}{RMS(\ddot{x}_{1a,U}(t))}$$
(4)

123   in which $x_{1,C}$ and $\ddot{x}_{1a,C}$ are the displacements and the absolute accelerations of the main structure of
124   the controlled system, while $x_{1,U}$ and $\ddot{x}_{1a,U}$ are the displacements and the absolute accelerations of the
125   uncontrolled system, respectively.
126   Two additional objective functions have been defined as the ratios of the maximum displacements
127   and absolute accelerations between the controlled and the uncontrolled systems:

128
$$\hat{J}_3 = \frac{\max(x_{1,C}(t))}{\max(x_{1,U}(t))}$$
(5)

129
$$\hat{J}_4 = \frac{\max(\ddot{x}_{1a,C}(t))}{\max(\ddot{x}_{1a,U}(t))}$$
(6)

130   The choice to minimise the dynamic response in terms of both displacements and accelerations was
131   made in order to take into account the structural integrity and safety of the structure, on one hand, and
132   the functionality of non-structural elements and comfort of occupants, on the other.
133
134   **3.1 Case Study**

135   In order to compare the four proposed objective functions, a case study has been selected as reference
136   structure based on a real small-scale experimental test [35]. The main structure is realised connecting
137   two steel columns through two nylon rigid plates, one of which is directly attached to a shaking table.
138   All the details of the primary structure are reported in Table 1. The cubic nonlinear stiffness is realised
139   by adopting the configuration proposed in reference [11]. The NES, attached to the top storey of the
140   system, is constituted by a small mass able to slide on a guide by means of a low friction car and
141   connected to the structure through a steel wire, with no pretension, located perpendicularly to the mass
142   motion direction.
143   In this first analysis, a mass ratio $\varepsilon = 0.05$ between the NES and the primary structure has been
144   considered. Gaussian random white noise samples, 20 seconds long, have been used as accelerations
145   to the base of the structure. It has been observed that increasing the duration of the base motion
146   time histories does not significantly affect the results.
147   A numerical searching technique has been used to identify the optimal values of the nonlinear
148   stiffness κ and the damping λ_2 of the NES. Monte Carlo Simulations (MCS) have been performed
149   using, for each analysis, 10000 base acceleration time histories with temporal sampling equal to 0.01 s
150   and modelled as samples of a Gaussian random white noises with a constant PSD function with
151   amplitude $S_0 = 10^{-3}$ $(m/s^2)^2/(rad/s)$, and directly integrating the nonlinear equations of motion by the
152   4th-order Runge-Kutta method. Each objective function, named J_i (i=1,…,4), has been obtained as
153   the average of the functions $\hat{J}_i$ (i=1,…,4), defined in eqs. (3)-(6), over the 10000 samples. A
154   preliminary analysis has been conducted to assess the accuracy of the MCS. 10000 samples have been

155 selected providing an estimated variation of the average results smaller than 0.1%. Figures 2a-b report
156 a sample of the white noise process and the one-side PSD of the white noise process ($G_0 = 2 \cdot S_0$)
157 reproduced using 10000 samples, respectively.

158   The variations of the four proposed objective functions with respect to the parameters κ and λ_2
159 are shown in Figure 3. A well-defined region of high effectiveness of the NES can be easily identified
160 for all cases. In fact, despite the values of the objective functions are different, the positions of their
161 minima in the search space are approximately the same in all four cases. Table 2 summarises the
162 optimal NES parameters for each objective function. Among them, the second one results the most
163 sensitive to variations of the parameters κ and λ_2. However, since the position of the minima is about
164 the same, in all the following analyses only J_1 will be considered in order to guarantee mainly the
165 structural integrity.

166   Because of the nonlinear behaviour of the coupled system, the numerical results of the optimisation
167 are strongly dependent on the selected structure and intensity of the excitation. In the following, two
168 methodologies are proposed to directly determine the optimal NES configuration. The first approach is
169 based on the Statistical Linearization Technique (SLT) allowing to derive two analytic, although
170 approximate formulae for the optimal NES parameters. The second one, instead, proposes high
171 accuracy empirical formulae based on the numerical results of a campaign of MCSs on several
172 different structures and white noise intensities.

173

174   4. OPTIMISATION OF THE NES PARAMETERS BY SLT

175 In this section, an approximate expression for the optimal NES parameters is obtained by linearizing
176 the system through the SLT and optimising it based on the linear TMD theory. Proposed firstly by
177 Caughey in reference [36], the SLT is an effective method to apply random vibration analysis on
178 systems with hysteretic nonlinear restoring forces [37]. In the last decades, approaches based on the
179 SLT have been proposed to study the performance of different passive control systems under random
180 loads [38–47].

181   For the nonlinear system described in section 2, the equations of motion (2) can be rewritten in
182 compact form as:

183

184     $\mathbf{M}\ddot{\mathbf{X}}(t) + \mathbf{C}\dot{\mathbf{X}}(t) + \mathbf{K}\mathbf{X}(t) + \mathbf{g}(\mathbf{X}(t)) = -\mathbf{M}\boldsymbol{\tau}\ddot{X}_g(t)$ (7)

185 where $\mathbf{X}(t) = \begin{bmatrix} X_1(t) & X_2(t) \end{bmatrix}^{\mathrm{T}}$ and the capital letters indicate stochastic processes; $\mathbf{M}$, $\mathbf{C}$ and $\mathbf{K}$ are
186 the mass, damping and linear stiffness matrices of the combined system, respectively:

187     $\mathbf{M} = \begin{bmatrix} 1 & 0 \\ 0 & \varepsilon \end{bmatrix}$; $\mathbf{C} = \begin{bmatrix} \lambda_1 + \lambda_2 & -\lambda_2 \\ -\lambda_2 & \lambda_2 \end{bmatrix}$; $\mathbf{K} = \begin{bmatrix} \omega_1^2 & 0 \\ 0 & 0 \end{bmatrix}$;   (8)

188 $\boldsymbol{\tau} = \begin{bmatrix} 1 & 1 \end{bmatrix}^{\mathrm{T}}$ is the location vector; and $\mathbf{g}(\mathbf{X}(t))$ is the following nonlinear vector:

189     $\mathbf{g}(\mathbf{X}(t)) = \kappa \begin{bmatrix} (X_1(t) - X_2(t))^3 \\ (X_2(t) - X_1(t))^3 \end{bmatrix}$ (9)

5

190 As shown in the previous section, the optimal parameters of the NES have been determined
191 minimising also the objective function J_1, defined in terms of RMS of the displacements of the
192 nonlinear system. This can be estimated, according to the SLT [48], by replacing the initial nonlinear
193 system with the following equivalent linear one:

194
$$\mathbf{M}\ddot{\mathbf{X}}(t) + \mathbf{C}\dot{\mathbf{X}}(t) + (\mathbf{K} + \mathbf{K}_e)\mathbf{X}(t) = -\mathbf{M}\boldsymbol{\tau}\ddot{X}_g(t) \tag{10}$$

195 in which $\mathbf{K}_e$ is the equivalent linear stiffness matrix, defined as:

196
$$\mathbf{K}_e = \varepsilon\omega_{2,e}^2 \begin{bmatrix} 1 & -1 \\ -1 & 1 \end{bmatrix} \tag{11}$$

197 The normalised equivalent linear stiffness $\varepsilon\omega_{2,e}^2$ can be determined minimising the mean square
198 error committed replacing eq. (7) with eq. (10), i.e.

199
$$E\left[\left(\mathbf{g}(\mathbf{x}(t)) - \mathbf{K}_e\mathbf{x}(t)\right)^T \left(\mathbf{g}(\mathbf{x}(t)) - \mathbf{K}_e\mathbf{x}(t)\right)\right] \rightarrow \min_{\varepsilon\omega_{2,e}^2} \tag{12}$$

200 where $E[\ \cdot\ ]$ indicates the ensemble average. By minimising this error, the normalised equivalent
201 stiffness is obtained as:

202
$$\varepsilon\omega_{2,e}^2 = 3\kappa E\left[\left(X_2(t) - X_1(t)\right)^2\right] \tag{13}$$

203 Since the response of the equivalent linear system excited by a zero-mean Gaussian process is a
204 zero-mean Gaussian process itself, eq. (13) can be rewritten as:

205
$$\omega_{2,e}^2 = 3\frac{\kappa}{\varepsilon}\sigma_{X_2-X_1}^2 = 3\frac{\kappa}{\varepsilon}\sigma_Y^2 \tag{14}$$

206 where σ_Y^2 is the variance of the relative displacements $Y = X_2 - X_1$ between the control device and the
207 main structure in the linearised system, and it can be computed as:

208
$$\sigma_Y^2 = \sigma_{X_1}^2 + \sigma_{X_2}^2 - 2\sigma_{X_1 X_2} \tag{15}$$

209 Since the base excitation is a white noise process, the steady-state variances can be determined in
210 closed-form by equating to zero the Lyapunov equation of the evolution of the covariance matrix [43]:

211
$$\mathbf{D}_s\boldsymbol{\Sigma}_\mathbf{Z}(t) + \boldsymbol{\Sigma}_\mathbf{Z}(t)\mathbf{D}_s^T + \mathbf{G}_s\mathbf{G}_s^T\pi S_0 = \dot{\boldsymbol{\Sigma}}_\mathbf{Z}(t) = \mathbf{0}$$
212
$$\tag{16}$$

213 where $\boldsymbol{\Sigma}_\mathbf{Z}(t)$ is the covariance matrix in terms of the state-space vector $\mathbf{Z} = \begin{bmatrix} \mathbf{X} & \dot{\mathbf{X}} \end{bmatrix}^T$, $\mathbf{D}_s$ and $\mathbf{G}_s$
214 are defined as:

215
$$\mathbf{D}_s = \begin{bmatrix} \mathbf{0} & \mathbf{I}_2 \\ -\mathbf{M}^{-1}(\mathbf{K} + \mathbf{K}_e) & -\mathbf{M}^{-1}\mathbf{C} \end{bmatrix}; \quad \mathbf{G}_s = \begin{bmatrix} \mathbf{0} \\ \mathbf{M}^{-1}\boldsymbol{\tau} \end{bmatrix} \tag{17}$$

216 and $\mathbf{I}_2$ is the 2 by 2 identity matrix. Eq. (16) leads to the following expression:

$$217 \qquad \sigma_Y^2 = \frac{\pi S_0 \omega_1}{2\omega_{2,e}^3 z} \tag{18}$$

218   in which the factor z is defined as:

$$219 \qquad z = \frac{\zeta_1\zeta_2\omega_1^4 + \left(\varepsilon + 4\zeta_1^2\right)\zeta_2^2\omega_1^3\omega_{2,e} + 2\zeta_1\zeta_2\left(-1 + 2\zeta_1^2 + 2(1+\varepsilon)\zeta_2^2\right)\omega_1^2\omega_{2,e}^2 + \zeta_1^2\left(\varepsilon + 4(1+\varepsilon)\zeta_2^2\right)\omega_1\omega_{2,e}^3 + (1+\varepsilon)^2\zeta_1\zeta_2\omega_{2,e}^4}{\zeta_1\omega_1^3 + \left(\varepsilon + 4\zeta_1^2\right)\zeta_2\omega_1^2\omega_{2,e} + \zeta_1\left(\varepsilon + 4\zeta_1^2 + 4(1+\varepsilon)\zeta_2^2\right)\omega_1\omega_{2,e}^2 + (1+\varepsilon)\left(1 + \varepsilon + 4\zeta_1^2\right)\zeta_2\omega_{2,e}^3}$$

$$220 \tag{19}$$

221   By substituting eq. (18) into eq. (14), the normalised NES nonlinear stiffness κ can be written as a
222   function of the linearised one as:

$$223 \qquad \kappa = \frac{2\varepsilon\omega_{2,e}^5 z}{3\pi S_0\omega_1} \tag{20}$$

224   The linear damping coefficient of the NES is instead equal to the damping of the linearised system:

$$225 \qquad \lambda_2 = 2\zeta_2\varepsilon\omega_{2,e} \tag{21}$$

226   Eqs. (20) and (21) can be exploited to determine the optimal NES design by using the linear TMD
227   theory, for which closed-form optimal solutions have been proposed in literature [49–51], depending
228   on the selected optimisation criteria, on the characteristics of the main structure and on the loading
229   conditions. The analytic solution proposed by Asami et al. [50] has been selected to optimise the
230   equivalent linear system for the case study introduced in section 3.1. This solution has been obtained
231   for random excitations, minimising the area under the frequency response function, i.e. the variance of
232   the displacements of the main structure. Hence, if the variances of the linear and nonlinear systems are
233   equal, Asami's optimisation criterion coincides with minimising the squared value of J_1. The solutions
234   selected for the determination of the optimum damping ratio $\zeta_{2,opt}$ and the optimum frequency ratio
235   v_{opt} are:

$$236 \qquad \zeta_{2,opt} = -\frac{\zeta_1}{v_{opt}}\frac{c_0 + c_1\zeta_1^2 + c_2\zeta_1^4 + c_3\zeta_1^6 + c_4\zeta_1^8 + c_5\zeta_1^{10} + c_6\zeta_1^{12}}{d_0 + d_1\zeta_1^2 + d_2\zeta_1^4 + d_3\zeta_1^6 + d_4\zeta_1^8 + d_5\zeta_1^{10} + c_6\zeta_1^{12}} \tag{22}$$

$$237 \qquad v_{opt} = \frac{\omega_{2,opt}}{\omega_1} = \sqrt{-\frac{p_2}{2} - \sqrt{\frac{p_2^2}{4} - q_2}} \tag{23}$$

238   in which the first parameter is function of the structural damping, mass ratio and optimum frequency
239   ratio, while the second one only depends on structural damping and mass ratio. For the determination
240   of the coefficient c_i, d_i, p_2 and q_2, readers should refer to [50]. Finally, substituting eqs. (22) and
241   (23) into (19)-(21), the optimal NES parameters are easily determined.
242   The accuracy of the results obtained using the proposed procedure has been assessed by
243   comparison with MCSs. In Table 3, the optimal NES stiffness and damping, normalised with respect
244   to the structural mass, are listed for assigned structural damping ratio ($\zeta_1 = \zeta_{1,R}$) and excitation
245   amplitude ($S_0 = 10^{-3}$ $(\text{m/s}^2)^2/(\text{rad/s})$) and for three different structural frequencies. The error

246 committed in estimating the NES optimal parameters has been computed using the following
247 expressions:

248
$$e_{\log_{10}\kappa} = \frac{\left|\log_{10}[\kappa_{opt,MCS}] - \log_{10}[\kappa_{opt,SLT}]\right|}{\left|\log_{10}[\kappa_{opt,MCS}]\right|}$$
(24)

249
$$e_{\lambda_2} = \frac{\left|\lambda_{2,opt,MCS} - \lambda_{2,opt,SLT}\right|}{\left|\lambda_{2,opt,MCS}\right|}$$
(25)

250 where $\kappa_{opt,MCS}$ and $\kappa_{opt,SLT}$ are the normalised nonlinear stiffness obtained through Monte Carlo
251 Simulations and through the formula (20), respectively; $\lambda_{2,opt,MCS}$ and $\lambda_{2,opt,SLT}$ are the normalised
252 NES damping coefficients obtained through Monte Carlo Simulations and through the formula (21),
253 respectively. As shown in Table 3, the error committed in the evaluation of the nonlinear stiffness (in
254 logarithmic scale) is below 5%, whereas for the NES damping is about 20%.
255 Figure 4 shows the J_1 values for the nonlinear system having parameters determined by eqs. (22)
256 and (23) versus the actual minimum of J_1, for three different values of the natural frequency of the
257 main structure. The following error function has been considered:

258
$$e_{J_1} = \frac{\left|J_{1,opt,MCS} - J_{1,opt,SLT}\right|}{\left|J_{1,opt,MCS}\right|}$$
(26)

259 where $J_{1,opt,MCS}$ and $J_{1,opt,SLT}$ are values of J_1 determined using the optimal NES parameters obtained
260 through the MCS and SLT, respectively. It can be noted that this error is less than 2%, as reported in
261 Table 3, and this confirms the robustness of the NES.
262 Although the NES is characterised by a strongly nonlinear stiffness term, this section showed how
263 the SLT approach still manages to return a quasi-optimal NES configuration in a stochastic sense.
264 Moreover, the proposed approach leads to analytic (although approximate) formulae for both NES
265 parameters, avoiding the computational effort required to perform the optimisation and Monte Carlo
266 simulation described into the previous section.
267

268 **5. EMPIRICAL FORMULAE FOR OPTIMAL NES PARAMETERS**

269 Since the SLT-based approach does not exactly predict the optimal NES parameters, a parametric
270 study has been conducted in order to obtain a more accurate design tool. In particular, the sensitivity
271 of the NES performance with respect to the intensity of the random excitation, the structural
272 frequency, the structural damping ratio and the mass ratio, has been analysed. The results have been
273 assessed against the results of Monte Carlo simulations and compared with those obtained by the first
274 proposed approach.
275

276 **5.1 Parametric Analysis**

277 Unlike linear vibration absorbers, the effectiveness of the NES is dependent on the intensity and type
278 of load on the main system. Hence, the optimal nonlinear stiffness, linking the device to the main
279 structure, has to be re-determined for any change on the white noise PSD amplitude.

280   Figure 5 shows how the objective function J_1 changes when the reference primary structure is
281   excited by white noise excitations whose PSD amplitude ranges between 10^{-4} and 10^{-2}
282    $(m/s^2)^2/(rad/s)$. These values have been selected in order to generate base acceleration peaks ranging
283   between 0.05 g and 1 g, corresponding to typical ground accelerations for civil engineering
284   applications. The general dynamic behaviour of the system does not change and a well-defined region
285   of effectiveness for each case can be identified in all considered cases. Although the objective function
286   maintains the same shape and value, it shifts in a direction parallel to the κ axis. Increasing values of
287   the amplitude of the PSD function of the white noise lead to decreasing optimal nonlinear stiffness, as
288   also proposed in [2]. Conversely, the normalised optimal damping λ_2, equal to 0.276 s^{-1}, is not
289   affected by the change in PSD amplitude S_0.

290   The optimal nonlinear stiffness coefficients κ, marked with red dots in Figure 6a, have been
291   reported in a log-log plot versus the amplitude of the white noise. These numerical results have been
292   numerically fitted using the following linear relationship (solid line) between the logarithms of the
293   optimal value of κ and S_0:

294
$$\log_{10} \kappa_{opt} = A \log_{10} S_0 + B \tag{27}$$

295   where κ_{opt} is the normalised optimal nonlinear stiffness expressed in $(m\ s)^{-2}$ and the coefficients A and
296   B, determined considering S_0 in $(m/s^2)^2/(rad/s)$, depend on the main structure parameters. For the
297   selected case study, A = -0.99 $(s/m^2)^2$ (rad/s) and B = 2.52 $(m\ s)^{-2}$ have been identified. Since the
298   analytic formula for the nonlinear stiffness based on the SLT, eq. (20), shows an inverse
299   proportionality between the nonlinear stiffness and the PSD amplitude, the value of A has been
300   rounded up to -1. For the considered case, the maximum difference between the values obtained
301   through numerical simulations and using eq. (27) is 0.04%. Analogous results have been obtained for
302   all the four proposed objective functions. Moreover, the authors verified that eq. (27) holds also for
303   PSD amplitudes larger than those reported in this paper.

304   A sensitivity analysis has been carried out in order to quantify the effects of the variation of the
305   primary structure parameters on the NES optimal design. The minimum J_1 has been determined for
306   several configurations of the primary structure, varying its frequency ω_1, damping ratio ζ_1 and the
307   mass ratio ε. The amplitude of the PSD function of the excitation process, S_0, has been varied as
308   described previously.

309   Figures 6a-b report the optimal κ_{opt} and $\lambda_{2,opt}$ against S_0 for five different values of ω_1 (selected
310   with respect to the frequency of the reference structure, $\omega_{1,R}$) and $\varepsilon = 0.05$. All the numerical
311   results, marked with different symbols, follow eq. (27). The optimal nonlinear stiffness, in fact,
312   decreases increasing S_0 while the optimal damping coefficient remains constant. Since fitting lines
313   obtained by eq. (27) are parallel, then the coefficient A is the same for any value of the main frequency
314   ω_1. Conversely, the coefficient B, increases for increasing ω_1.

315   Analogously, the dependence of the optimal NES parameters on the structural damping ratio ζ_1
316   (selected with respect to the damping ratio of the reference structure, $\zeta_{1,R}$) has been investigated, as
317   shown in Figures 7a-b. Numerical results confirm again the validity of eq. (27). The coefficient A is
318   independent on the damping ratio ζ_1 and the coefficient B increases for increasing damping ratio of
319   the primary structure.

320   Finally, Figures 8a-b show the effects of the variation of the amplitude of the white noise excitation
321   on the optimal parameters κ_{opt} and $\lambda_{2,opt}$ for different values of the mass ratio ε. The assumption of
322   lightweight NES has been introduced not only to trigger the passive target energy transfer, that occurs

323 for small values of the mass of the NES, but also for practical issues related to the costs and realisation
324 of the system. For this reason, the values of the mass ratio ε considered in the analysis have been set
325 at 0.025, 0.05 and 0.1. The optimal nonlinear stiffness, inversely proportional to the amplitude of the
326 PSD function, increases also increasing the mass ratio.
327   With regards to the normalised optimal NES damping $\lambda_{2,opt}$, the latter increases increasing the
328 main frequency of the primary structure as well as the mass ratio and decreasing the structural
329 damping ratio, as shown in Figures 6b, 7b and 8b. The optimal NES parameters and the corresponding
330 values of the J_1 are listed in Table 4 for the case of $\varepsilon = 0.05$ and $S_0 = 10^{-3}\,(\text{m/s}^2)^2/(\text{rad/s})$.
331

5.2 Optimal nonlinear stiffness and damping of the NES

333 Extending the parametric analysis to several combinations of ω_1, ζ_1, S_0 and ε, and fitting all the
334 numerical results, the following empirical formulae for the nonlinear stiffness $[(\text{m s})^{-2}]$ and damping
335 $[\text{s}^{-1}]$ of the NES have been obtained:

337
$$\log_{10}\kappa_{opt} = -\log_{10} S_0 + 4.98\log_{10}\omega_1 + 0.21\log_{10}\zeta_1 + 1.33\log_{10}\varepsilon - 1.908 \tag{28}$$

338
$$\lambda_{2,opt} = (0.204\varepsilon - 0.001)\zeta_1^{-0.1}\omega_1 \tag{29}$$

339 where the coefficients have been determined considering S_0 expressed in $(\text{m/s}^2)^2/(\text{rad/s})$ and ω_1 in
340 rad/s.
341   Eqs. (28) and (29) are graphically represented in Figures 9a-c as function of frequency and
342 damping ratio of the main structure. In particular, Figure 9a shows the dependence of the optimal
343 nonlinear stiffness on the PSD function amplitude for $\varepsilon = 0.05$, whereas Figure 9b shows its
344 dependence on the mass ratio for $S_0 = 10^{-3}\,(\text{m/s}^2)^2/(\text{rad/s})$. κ_{opt} increases with the frequency and
345 damping of the primary structure, yet it is more sensitive to the former than the latter.
346   The optimal damping ratio $\lambda_{2,opt}$ does not depend on the intensity of the excitation. Conversely, its
347 dependence on the mass ratio is reported in Figure 9c. The NES damping is directly proportional to the
348 structural frequency and mass ratio and decreases for increasing structural damping ratio.
349   Taking advantage of eqs. (28) and (29), optimal design charts can be created for the evaluation of
350 the NES parameters. Examples are shown in Figures 10-12, for three values of the mass ratio. These
351 diagrams allow to quickly determine the optimal NES parameters for assigned main structure
352 (frequency and damping) and selected mass ratio and intensity of the random excitation.
353   The error (with respect to MCSs), committed estimating the optimal parameters and the function
354 J_1 using the SLT-based approach and the proposed empirical formulae, has been determined varying
355 the involved parameters (ω_1, ζ_1, S_0 and ε). These errors are shown in Figures 13-15 for the case of
356 mass ratio $\varepsilon = 0.05$ and for three values of the PSD amplitude.
357   For the optimal nonlinear stiffness, the error increases with the PSD amplitude, however the
358 absolute error does not change. The maximum error is obtained for $S_0 = 10^{-3}\,(\text{m/s}^2)^2/(\text{rad/s})$ and it is
359 equal to 16.84% using the SLT-based approach, while only 3.53% using the empirical one.
360   Otherwise, the errors in terms of $\lambda_{2,opt}$ and J_1 determined using both the proposed approaches are
361 approximately the same for each values of S_0, as shown in Figures 14-15. In fact, the NES damping
362 and the minimum value of J_1 do not depend on the amplitude of the excitation, as previously shown in
363 Figure 5. For the optimal NES damping, the SLT-based approach can produce significant errors, with

364   a maximum error (for the studied case) of 32.5%. Conversely, by using the empirical formula the error
365   is below 5.5% for all the values of structural frequency and damping ratio except for the case of
366   $\omega_1 = 4\,\omega_{1,R}$ and $\zeta_1 = 2\,\zeta_{1,R}$ in which the error is 13.9%. Finally, the maximum error in terms of J_1 is
367   4% for the SLT-based approach, versus only 0.86% for the empirical approach.

368   Although it is not statistically significant, a sample of the response process of the reference
369   structure (Table 1) is presented in Figures 16a-b in order to show the effectiveness of the optimised
370   NES with the proposed empirical formulae (28) and (29). In particular, a comparison between the
371   uncontrolled (i.e. removing the NES) and controlled (i.e. with attached NES) configurations, in terms
372   of relative displacements to the base (Figure 16a) and of absolute accelerations (Figure 16b) of the
373   primary structure is showed. Initially, the NES does not work properly because it undergoes small
374   oscillations and most of the input energy is localised to the primary structure. The reduction of the
375   response occurs when the level of the motion increases, i.e. when the motion is strongly localised in
376   the NES thus activating the energy pumping from the primary system, as shown in Figures 16c-d.
377   Furthermore, Figures 16e-f report the comparison between the two configurations in the frequency-
378   domain in terms of the PSD of the response process. These show that the NES is an effective passive
379   control device and it is capable to guarantee the requirements of structural integrity and comfort.

6. SIMPLIFIED DESIGN OF NESs FOR MULTI-DOF STRUCTURES: A NUMERICAL APPLICATION

382   Although the numerical formulae presented in this work have been obtained only on the base of SDOF
383   models, they can be adopted for MDOF structures for an approximate simplified design of NESs. In
384   this section, the dynamic response of a 2-DOF linear system coupled with a NES, optimised by means
385   of eqs. (28) and (29), has been investigated. A schematic diagram of this system is reported in Figure
386   17. A case study has been selected based on a 2-DOF physical experimental model utilised in the
387   Smart Structure Technology Laboratory at the University of Illinois at Urbana-Champaign [2,14,52].
388   The lumped masses are 24.3 and 24.2 kg for the first and second storeys, respectively; the stiffnesses
389   are 6820 and 8220 N/m for the first and second storeys, respectively, and the damping of the model is
390   set at 2% at each mode. The resulting natural frequencies of this structure are 10.62 and 29.09 rad/s for
391   the first and second modes, respectively. The equations of motion of the 2-DOF structure in its
392   uncontrolled configuration are:

393
$$\begin{cases} m_1\ddot{x}_1 + c_1\dot{x}_1 + k_1 x_1 + c_2\left(\dot{x}_1 - \dot{x}_2\right) + k_2\left(x_1 - x_2\right) = -m_1\ddot{x}_g \\ m_2\ddot{x}_2 + c_2\left(\dot{x}_2 - \dot{x}_1\right) + k_2\left(x_2 - x_1\right) = -m_2\ddot{x}_g \end{cases} \tag{30}$$

394   in which m_i, c_i, k_i and x_i (i = 1,2) are respectively mass, viscous damping coefficient, stiffness
395   coefficient and displacement relative to the base of the i-th storey, and $\ddot{x}_g$ is the base acceleration
396   modelled as a zero-mean stationary Gaussian white noise, with PSD amplitude S_0. The equations of
397   motion of the 2-DOF system combined with an ungrounded NES (i.e. controlled configuration) can be
398   written as:

399
$$\begin{cases} m_1\ddot{x}_1 + c_1\dot{x}_1 + k_1 x_1 + c_2\left(\dot{x}_1 - \dot{x}_2\right) + k_2\left(x_1 - x_2\right) = -m_1\ddot{x}_g \\ m_2\ddot{x}_2 + c_2\left(\dot{x}_2 - \dot{x}_1\right) + k_2\left(x_2 - x_1\right) + c_N\left(\dot{x}_2 - \dot{x}_N\right) + k_N\left(x_2 - x_N\right)^3 = -m_2\ddot{x}_g \\ m_N\ddot{x}_N + c_N\left(\dot{x}_N - \dot{x}_2\right) + k_N\left(x_N - x_2\right)^3 = -m_N\ddot{x}_g \end{cases} \tag{31}$$

400 where m_N, c_N, k_N and x_N are mass, viscous damping coefficient, stiffness coefficient and
401 displacement relative to the base of the NES.

402   The design of the NES has been carried out by considering a SDOF structure with mass equivalent
403 to the effective modal mass at the first mode of the original structure ($m_{1,e} = 46.65$ kg), frequency
404 $\omega_1 = 10.62$ rad/s (the first modal frequency) and damping 2%. Therefore, applying eqs. (28) and (29)
405 for $S_0 = 10^{-3}$ (m/s²)²/(rad/s), $\omega_1 = 10.62$ rad/s, $\zeta_1 = 0.02$ and $\varepsilon = 0.05$, the NES optimal parameters
406 has been directly determined, i.e.:

407

$$m_N = 0.05 \cdot m_{1,e} = 2.33 \text{ kg}$$

408
$$k_N = \kappa_{opt} \cdot m_{1,e} = 10^{5.78} \text{ N/m}^3 \qquad\qquad (32)$$

$$c_N = \lambda_{2,opt} \cdot m_{1,e} = 6.74 \text{ Ns/m}$$

409   The accuracy of the results has been assessed by comparison with MCSs. The latter have been
410 performed using 10000 base acceleration time histories, modelled as samples of a Gaussian random
411 white noise and directly integrating the nonlinear equations of motion by the 4th-order Runge-Kutta
412 method. Two objective functions J_1 and J_2, based on the ratio of the RMS of the displacements of the
413 two storeys in their controlled and uncontrolled configurations, have been selected for the optimisation
414 problem. These have been obtained by averaging the following functions over the generated 10000
415 samples:

416
$$\hat{J}_1 = \frac{RMS(x_{1,C}(t))}{RMS(x_{1,U}(t))} \qquad\qquad (33)$$

417
$$\hat{J}_2 = \frac{RMS(x_{2,C}(t))}{RMS(x_{2,U}(t))} \qquad\qquad (34)$$

418 in which $\hat{J}_1$ and $\hat{J}_2$ are defined for a single sample of base acceleration time-history; $x_{1,C}$ and $x_{2,C}$ are
419 the displacements of the first and second floors of the controlled system, while $x_{1,U}$ and $x_{2,U}$ are the
420 displacements of the first and second floors of the uncontrolled system, respectively.
421   Figures 18a-b show J_1 and J_2 values for the nonlinear system having parameters determined by
422 eqs. (28) and (29) (marked with red dots) versus the actual minima of J_1 and J_2 obtained by MCSs
423 (marked with black dots). It can be noted that the error committed on the reduction of the RMS of the
424 displacements of the primary structure is less than 1%.
425   The dampening effects of the NES (optimised by using the proposed empirical formulation) are
426 shown, for a single sample of the response of the system in its controlled and uncontrolled
427 configurations, in terms of displacements of the two storeys (Figures 19a-b). Since the optimisation
428 approach is defined in a stochastic framework, results in the frequency-domain are shown in terms of
429 the PSD of the 10000 samples of response determined by the MCS (Figure 19c-d), instead of just the
430 Fourier spectrum of the response of a single sample. The comparison in the frequency-domain in terms
431 of PSD of response process shows a considerable reduction of the response at the first mode.
432   The proposed simplified optimisation procedure for the NES works well for MDOF systems
433 dominated by one mode, as, for example, in the case of high-rise buildings. Hence, the higher the
434 effective modal mass at that mode, the better the performance of the NES is. Further investigation on

435 the interaction between modes and on the most appropriate objective functions to minimise is required
436 to overcome this limitation.

437

438 **CONCLUSIONS**

439 In this paper, the optimal design of an ungrounded NES attached to a SDOF structure excited by a
440 stationary Gaussian white noise process has been investigated. Two design approaches have been
441 presented in order to reduce the computational burden required to perform a numerical optimisation.

442 In the first case, an analytic procedure based on the Statistical Linearization Technique and the
443 TMD theory has been proposed. The optimal nonlinear stiffness has been obtained by minimising the
444 mean square error between the nonlinear system and the linearised one with respect to its structural
445 parameters. Accordingly, a relationship between the parameters of the NES and its linear equivalent
446 system has been determined. The latter acts as a TMD, whose optimal parameters (i.e. those
447 minimising the RMS of the response of the main structure) are known in closed-form in literature.
448 Hence, by inverse process, the NES optimal parameters are determined by first opportunely tuning its
449 equivalent system, and then exploiting the relationships between the structural parameters of both
450 linear and nonlinear systems. Although this method does not predict the exact optimal NES
451 parameters, it returns a quasi-optimal design of the NES. For the analysed case study, the maximum
452 error estimated on the reduction of the RMS of the displacements of the primary structure (used as a
453 measure of the NES effectiveness) does not exceed 3.6%.

454 The second approach is fully numerical and provides empirical formulae that can be
455 straightforwardly used to determine the optimal NES parameters. For this purpose, a parametric study
456 with respect to the intensity of the random excitation, the structural frequency, the structural damping
457 ratio and the mass ratio, has been performed using Monte Carlo Simulations. By a curve fitting
458 procedure of the optimal NES parameters obtained for several configurations of the main system,
459 empirical formulae for the optimal NES stiffness and damping have been derived for any primary
460 structure and any random load intensity. These formulae allow for a significant reduction of the error
461 committed in the evaluation of the optimal parameters of the NES with respect to the first approach.
462 The easy implementation of the formulae entails also a reduced computational effort, making the
463 method suitable for practical engineering purposes. With this aim, it has been shown how the proposed
464 empirical formulae can be easily translated in optimal NES design charts.

465 The sensitivity of the optimal NES parameters with respect to the above mentioned parameters has
466 been widely investigated. In particular, it has been demonstrated that the optimal nonlinear stiffness is
467 inversely proportional to the amplitude of the PSD function of the white noise, yet it increases with the
468 parameters of the main structure (frequency and damping ratio) as well as the mass ratio between the
469 NES and the primary structure. The optimal NES damping, instead, is independent from the amplitude
470 of the white noise, increases for increasing structural frequency and mass ratio and for decreasing
471 damping ratio of the primary structure.

472 Finally, the applicability of the proposed approach to MDOF structures has been shown through a
473 numerical application on a 2DOF model. The optimal NES parameters in this case are obtained by
474 considering an equivalent SDOF structure, whose structural parameters are based on the effective
475 modal mass at the first mode of vibrations. The proposed design methodology works well for MDOF

13

476 systems dominated by one mode (e.g. high-rise buildings) and further studies are required to overcome
477 this limitation.
478

479 **REFERENCES**

480 [1] Housner GW, Bergman LA, Caughey TK, Chassiakos AG, Claus RO, Masri SF, et al. Structural
481   Control : Past , Present and Future. J Eng Mech 1997;123:897–971.
482 [2] Wierschem NE, Spencer Jr BF, Bergman LA, Vakakis AF. Numerical study of nonlinear energy sinks
483   for seismic response reduction. Proc. 6th Int. Work. Adv. Smart Mater. Smart Struct. Technol., 2011.
484 [3] Gendelman O, Manevitch LI, Vakakis AF, M'Closkey R. Energy pumping in nonlinear mechanical
485   oscillators: Part I—Dynamics of the underlying hamiltonian systems. J Appl Mech 2001;68:34.
486 [4] Vakakis AF, Gendelman OV. Energy pumping in nonlinear mechanical oscillators: Part II—Resonance
487   Capture. J Appl Mech 2001;68:42.
488 [5] Kerschen G, Lee YS, Vakakis A., McFarland DM, Bergman LA. Irreversible passive energy transfer in
489   coupled oscillators with essential nonlinearity. SIAM J Appl Math 2005;66:648–79.
490 [6] Lee YS, Kerschen G, Vakakis AF, Panagopoulos P, Bergman L, McFarland DM. Complicated dynamics
491   of a linear oscillator with a light, essentially nonlinear attachment. Phys D Nonlinear Phenom
492   2005;204:41–69.
493 [7] Gendelman OV. Transition of energy to a nonlinear localized mode in a highly asymmetric system of
494   two oscillators. Nonlinear Dyn 2001;25:237–53.
495 [8] Vakakis AF, Gendelman OV, Bergman LA, McFarland DM, Kerschen G, Lee YS. Nonlinear targeted
496   energy transfer in mechanical and structural systems. vol. 156. Dordrecht: Springer Netherlands; 2009.
497 [9] Nucera F, Vakakis AF, McFarland DM, Bergman LA, Kerschen G. Targeted energy transfers in vibro-
498   impact oscillators for seismic mitigation. Nonlinear Dyn 2007;50:651–77.
499 [10] Nucera F, Lo Iacono F, McFarland DM, Bergman LA, Vakakis AF. Application of broadband nonlinear
500   targeted energy transfers for seismic mitigation of a shear frame: Experimental results. J Sound Vib
501   2008;313:57–76.
502 [11] McFarland DM, Bergman LA, Vakakis AF. Experimental study of non-linear energy pumping occurring
503   at a single fast frequency. Int J Non Linear Mech 2005;40:891–9.
504 [12] Kerschen G, McFarland DM, Kowtko JJ, Lee YS, Bergman LA, Vakakis AF. Experimental
505   demonstration of transient resonance capture in a system of two coupled oscillators with essential
506   stiffness nonlinearity. J Sound Vib 2007;299:822–38.
507 [13] Gourdon E, Alexander NA, Taylor CA, Lamarque CH, Pernot S. Nonlinear energy pumping under
508   transient forcing with strongly nonlinear coupling: Theoretical and experimental results. J Sound Vib
509   2007;300:522–51.
510 [14] Wang J, Wierschem NE, Spencer BF, Lu X. Track Nonlinear energy sink for rapid response reduction in
511   building structures. J Eng Mech 2015;141:4014104.
512 [15] Lee YS, Vakakis AF, Bergman LA, McFarland DM, Kerschen G, Nucera F, et al. Passive non-linear
513   targeted energy transfer and its applications to vibration absorption: a review. Proc. Inst. Mech. Eng. Part
514   K J. Multi-body Dyn., vol. 222, 2008, p. 77–134.
515 [16] Vakakis AF. Inducing passive nonlinear energy sinks in vibrating systems. J Vib Acoust 2001;123:324..
516 [17] Wang J, Wierschem N, Spencer BF, Lu X. Experimental study of track nonlinear energy sinks for
517   dynamic response reduction. Eng Struct 2015;94:9–15.
518 [18] Gourc E, Michon G, Seguy S, Berlioz A. Experimental investigation and design optimization of targeted
519   energy transfer under periodic forcing. J Vib Acoust 2014;136:21021.
520 [19] Jiang X, McFarland DM, Bergman LA, Vakakis AF. Steady state passive nonlinear energy pumping in
521   coupled oscillators: theoretical and experimental results. Nonlinear Dyn 2003;33:87–102.
522 [20] Gendelman OV, Gourdon E, Lamarque CH. Quasiperiodic energy pumping in coupled oscillators under
523   periodic forcing. J Sound Vib 2006;294:651–62.
524 [21] Starosvetsky Y, Gendelman OV. Response regimes of linear oscillator coupled to nonlinear energy sink
525   with harmonic forcing and frequency detuning. J Sound Vib 2008;315:746–65.
526 [22] Luo J, Wierschem NE, Hubbard SA, Fahnestock LA, Quinn DD, McFarland DM, et al. Large-scale
527   experimental evaluation and numerical simulation of a system of nonlinear energy sinks for seismic
528   mitigation. Eng Struct 2014;77:34–48.
529 [23] Manevitch L., Gourdon E, Lamarque CH. Towards the design of an optimal energetic sink in a strongly
530   inhomogeneous two-degree-of-freedom system. J Appl Mech 2007;74:1078.

531 [24] Manevitch LI, Gendelman O, Musienko AI, Vakakis AF, Bergman L. Dynamic interaction of a semi-
532 infinite linear chain of coupled oscillators with a strongly nonlinear end attachment. Phys D Nonlinear
533 Phenom 2003;178:1–18.
534 [25] Starosvetsky Y, Gendelman O V. Attractors of harmonically forced linear oscillator with attached
535 nonlinear energy sink. II: Optimization of a nonlinear vibration absorber. Nonlinear Dyn 2008;51:47–57.
536 [26] Vaurigaud B, Ture Savadkoohi A, Lamarque CH. Targeted energy transfer with parallel nonlinear
537 energy sinks. Part I: Design theory and numerical results. Nonlinear Dyn 2011;66:763–80.
538 [27] Nguyen TA, Pernot S. Design criteria for optimally tuned nonlinear energy sinks—part 1: transient
539 regime. Nonlinear Dyn 2012;69:1–19.
540 [28] Boroson E, Missoum S. Reliability-based design optimization of nonlinear energy sinks. 11th World
541 Congr. Struct. Multidiscip. Optim., 2015, p. 750–7.
542 [29] Younesian D, Nankali A, Motieyan E. Optimal nonlinear energy sinks in vibration mitigation of the
543 beams traversed by successive moving loads. J Solid Mech 2011;3:323–31.
544 [30] Parseh M, Dardel M, Ghasemi MH. Investigating the robustness of nonlinear energy sink in steady state
545 dynamics of linear beams with different boundary conditions. Commun Nonlinear Sci Numer Simul
546 2015;29:50–71.
547 [31] Wierschem NE, Luo J, Hubbard S, Fahnestock LA, Spencer, Jr. BF, Vakakis AF, et al. Experimental
548 Testing of a Large 9-Story Structure Equipped with Multiple Nonlinear Energy Sinks Subjected to an
549 Impulsive Loading. Struct. Congr. 2013, 2013, p. 2241–52
550 [32] Spencer, Jr. BF, Christenson RE, Dyke SJ. Next generation benchmark control problem for seismically
551 excited buildings. Proc. Second World Conf. Struct. Control, vol. 2, New York: Wiley; 1999, p. 1135–
552 1360.
553 [33] Ohtori Y, Christenson RE, Spencer BF, Dyke SJ. Benchmark control problems for seismically excited
554 nonlinear buildings. J Eng Mech 2004:366–85.
555 [34] Nucera F, McFarland DM, Bergman LA, Vakakis AF. Application of broadband nonlinear targeted
556 energy transfers for seismic mitigation of a shear frame: Computational results. J Sound Vib
557 2010;329:2973–94.
558 [35] Lo Iacono F. Passive control strategies for seismically excited structures. Theoretical and experimental
559 analisys. PhD Thesis, Mediterranean University of Reggio Calabria, Reggio Calabria, Italy, 2008.
560 [36] Caughey TK. Equivalent linearization techniques. J Acoust Soc Am 1963;35:1706–11.
561 [37] Spanos PD. Stochastic linearization in structural dynamics. Appl Mech Rev 1981;34:1–8.
562 [38] Pandey MD. Stochastic analysis of structures with passive seismic control. Can J Civ Eng 1995;22:970–
563 80.
564 [39] Won AYJ, Pires JA, Haroun MA. Performance assessment of tuned liquid column dampers under
565 random seismic loading. Int J Non Linear Mech 1997;32:745–58.
566 [40] Yalla SK, Kareem A. Optimum absorber parameters for tuned liquid column dampers. J Struct Eng
567 2000;126:906–15.
568 [41] Socha L. Linearization in analysis of nonlinear stochastic systems: recent results—Part I: Theory. Appl
569 Mech Rev 2005;58:178.
570 [42] Socha L. Linearization in analysis of nonlinear stochastic systems, recent results—Part II: applications.
571 Appl Mech Rev 2005;58:303.
572 [43] Di Matteo A, Lo Iacono F, Navarra G, Pirrotta A. Direct evaluation of the equivalent linear damping for
573 TLCD systems in random vibration for pre-design purposes. Int J Non Linear Mech 2014;63:19–30.
574 [44] Di Matteo A, Lo Iacono F, Navarra G, Pirrotta A. Optimal tuning of tuned liquid column damper
575 systems in random vibration by means of an approximate formulation. Meccanica 2015;50:795–808.
576 [45] Guo AX, Xu XL, Wu B. Seismic reliability analysis of hysteretic structure with viscoelastic dampers.
577 Eng Struct 2002;24:373–83.
578 [46] Di Paola M, La Mendola L, Navarra G. Stochastic seismic analysis of structures with nonlinear viscous
579 dampers. J Struct Eng 2007;133:1475–8.
580 [47] Di Paola M, Navarra G. Stochastic seismic analysis of MDOF structures with nonlinear viscous
581 dampers. Struct Control Heal Monit 2009;16:303–18.
582 [48] Atalik TS, Utku S. Stochastic linearization of multi-degree-of-freedom non-linear systems. Earthq Eng
583 Struct Dyn 1976;4:411–20.
584 [49] Warburton GB. Optimum absorber parameters for minimizing vibration response. Earthq Eng Struct
585 Dyn 1981;9:251–62.
586 [50] Asami T, Nishihara O, Baz AM. Analytical Solutions to H_∞ and H_2 Optimization of Dynamic Vibration
587 Absorbers Attached to Damped Linear Systems. J Vib Acoust 2002;124:284.
588 [51] Ghosh A, Basu B. A closed-form optimal tuning criterion for TMD in damped structures. Struct Control

589 Heal Monit 2007;14:681–92.

590 [52] Wierschem NE, Quinn DD, Hubbard SA, Al-Shudeifat MA, McFarland DM, Luo J, et al. Passive

591   damping enhancement of a two-degree-of-freedom system through a strongly nonlinear two-degree-of-

592   freedom attachment. J Sound Vib 2012;331:5393–407.

593

Table 1: Characteristics of the reference main structure.

$m_{1,R}$	$c_{1,R}$	$k_{1,R}$	$f_{1,R}$	$\omega_{1,R}$	$\zeta_{1,R}$
[Ns^2/m]	[Ns/m]	[N/m]	[Hz]	[rad/s]	[%]
2.135	1.57	890	3.25	20.42	1.8

Table 2: Optimal parameters of the NES coupled to the reference main structure for $S_0 = 10^{-3}$ $(\text{m/s}^2)^2/(\text{rad/s})$.

	$\lambda_{2,opt}$	κ_{opt}
	$[\text{s}^{-1}]$	$[(\text{s m})^{-2}]$
J_1	0.276	$10^{5.52}$
J_2	0.278	$10^{5.60}$
J_3	0.29	$10^{5.52}$
J_4	0.29	$10^{5.60}$

Table 3: Comparison between the optimal parameters obtained through the MCS and through the SLT for $S_0 = 10^{-3}$ $(m/s^2)^2/(rad/s)$.

		MCS			SLT			Errors		
ω_1	ζ_1	$\lambda_{2,opt}$	$\log_{10}[\kappa_{opt}]$	J_1	$\lambda_{2,opt}$	$\log_{10}[\kappa_{opt}]$	J_1	e_{λ_2}	$e_{\log_{10}\kappa}$	e_{J_1}
[rad/s]	[%]	[s^{-1}]	[(s m)$^{-2}$]	[-]	[s^{-1}]	[(s m)$^{-2}$]	[-]	[%]	[%]	[%]
$2\,\omega_{1,R}$	$\zeta_{1,R}$	0.55	7.02	0.649	0.43	6.83	0.659	21.82	2.71	1.54
$\omega_{1,R}$	$\zeta_{1,R}$	0.276	5.52	0.664	0.22	5.32	0.675	20.29	3.62	1.66
$0.5\,\omega_{1,R}$	$\zeta_{1,R}$	0.14	4.02	0.693	0.11	3.82	0.706	21.43	4.98	1.88

Table 4: Optimal NES parameters for $S_0 = 10^{-3} \, \text{(m/s}^2)^2/\text{(rad/s)}$ and $\varepsilon = 0.05$.

			$0.25\,\zeta_{1,R}$	$0.5\,\zeta_{1,R}$	$\zeta_{1,R}$	$2\,\zeta_{1,R}$	$4\,\zeta_{1,R}$
$0.25\,\omega_{1,R}$	$\lambda_{2,opt}$	$[\text{s}^{-1}]$	0.08	0.075	0.069	0.064	0.060
	$\log_{10}[\kappa_{opt}]$	$[(\text{s m})^{-2}]$	2.40	2.50	2.53	2.62	2.69
	J_1	$[\text{-}]$	0.65	0.69	0.74	0.81	0.89
$0.5\,\omega_{1,R}$	$\lambda_{2,opt}$	$[\text{s}^{-1}]$	0.16	0.15	0.14	0.13	0.12
	$\log_{10}[\kappa_{opt}]$	$[(\text{s m})^{-2}]$	3.90	3.96	4.02	4.09	4.13
	J_1	$[\text{-}]$	0.55	0.61	0.69	0.79	0.88
$\omega_{1,R}$	$\lambda_{2,opt}$	$[\text{s}^{-1}]$	0.305	0.293	0.275	0.262	0.243
	$\log_{10}[\kappa_{opt}]$	$[(\text{s m})^{-2}]$	5.40	5.46	5.52	5.58	5.65
	J_1	$[\text{-}]$	0.48	0.56	0.66	0.78	0.88
$2\,\omega_{1,R}$	$\lambda_{2,opt}$	$[\text{s}^{-1}]$	0.61	0.58	0.55	0.37	0.35
	$\log_{10}[\kappa_{opt}]$	$[(\text{s m})^{-2}]$	6.93	6.96	7.02	7.08	7.16
	J_1	$[\text{-}]$	0.43	0.53	0.65	0.77	0.87
$4\,\omega_{1,R}$	$\lambda_{2,opt}$	$[\text{s}^{-1}]$	1.25	1.20	1.105	0.95	0.94
	$\log_{10}[\kappa_{opt}]$	$[(\text{s m})^{-2}]$	8.43	8.46	8.52	8.59	8.65
	J_1	$[\text{-}]$	0.47	0.56	0.66	0.78	0.87
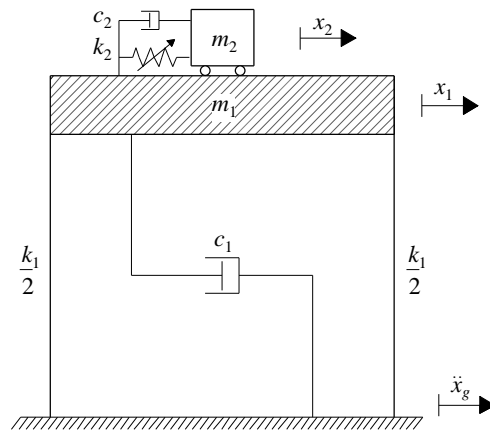
Figure 1: SDOF structure coupled with a NES.

(a)

(b)
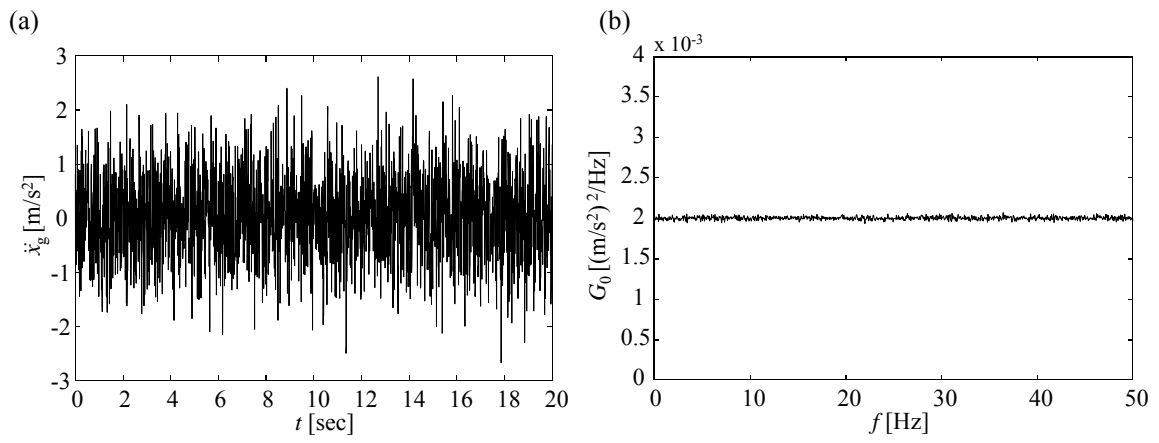
Figure 2: a) a sample of white noise process; b) one-side PSD of the white noise process.
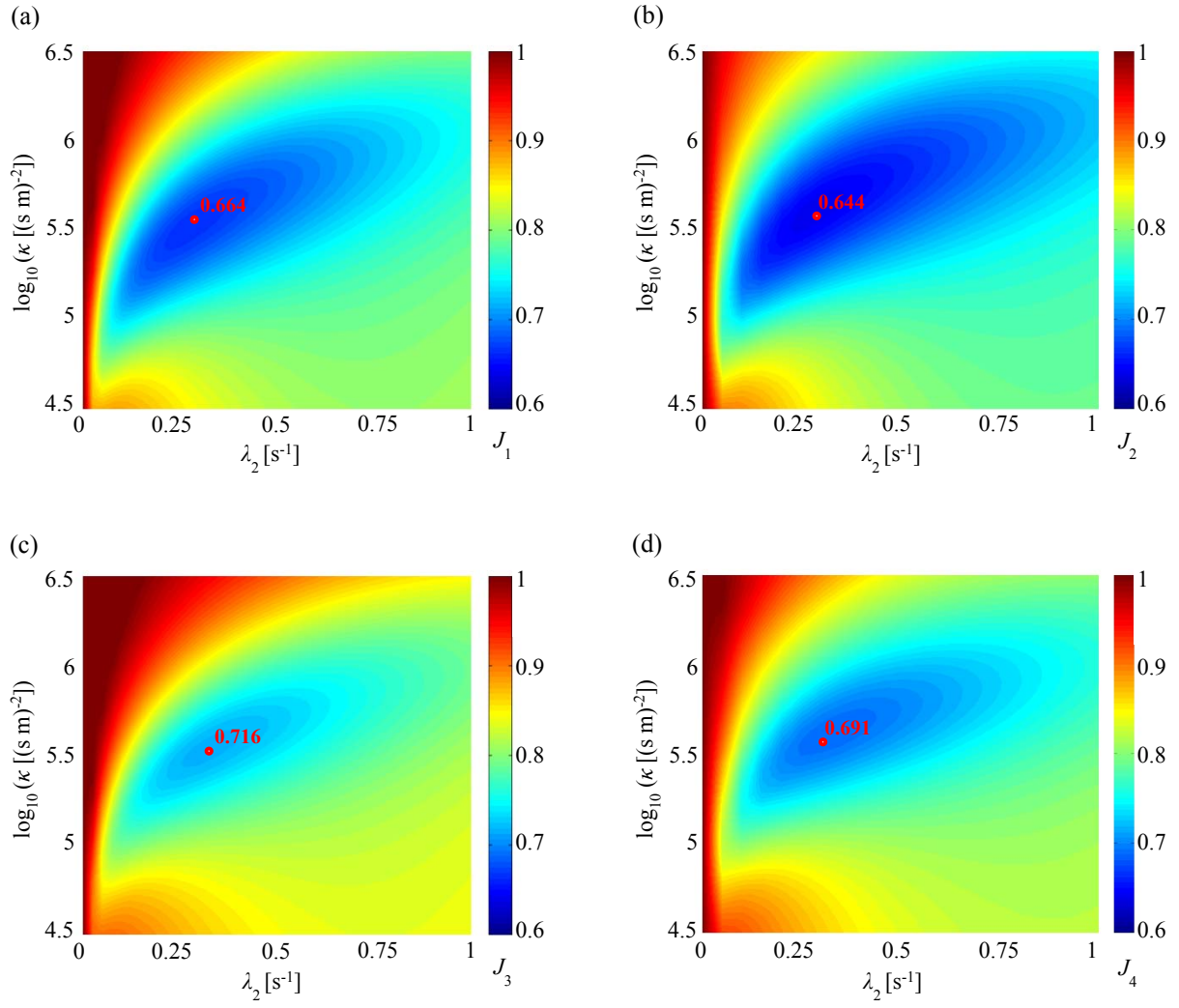
Figure 3: Objective functions with respect to the normalised NES parameters κ and λ_2: a) J_1; b) J_2; c) J_3; d) J_4.
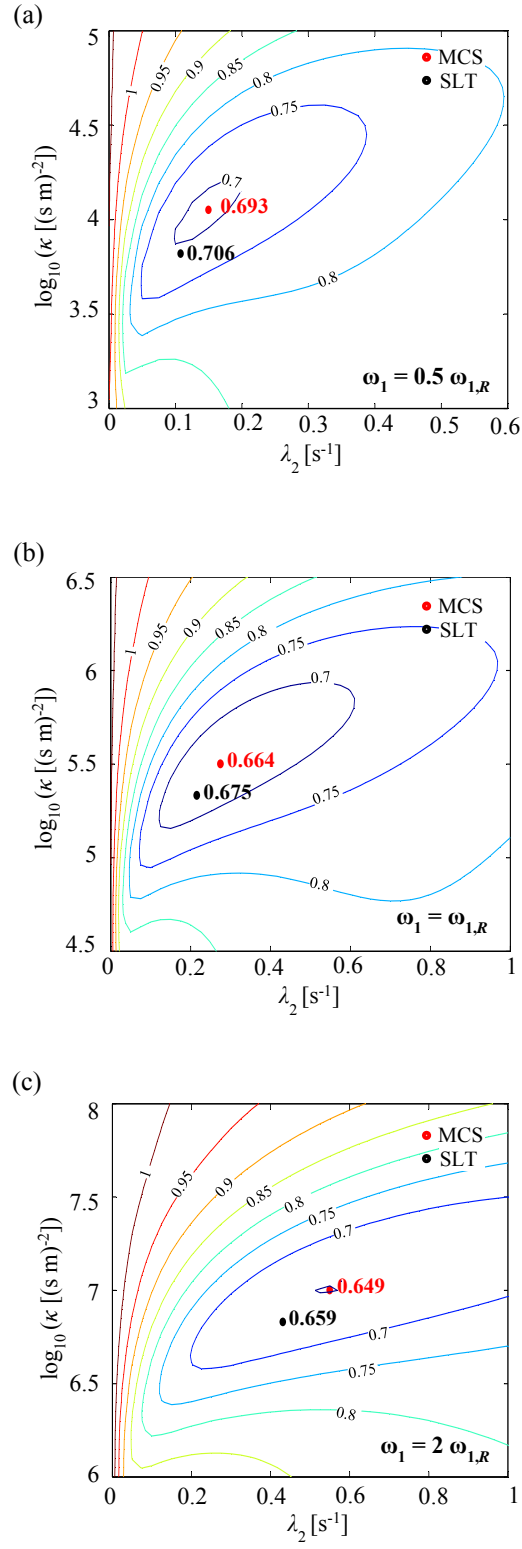
Figure 4: J_1 function and optimal NES parameters obtained by MCS (red dot) and SLT (black dot) for $S_0 = 10^{-3}$ (m/s²)²/(rad/s).

(a)

(b)

(c)

(d)

(e)
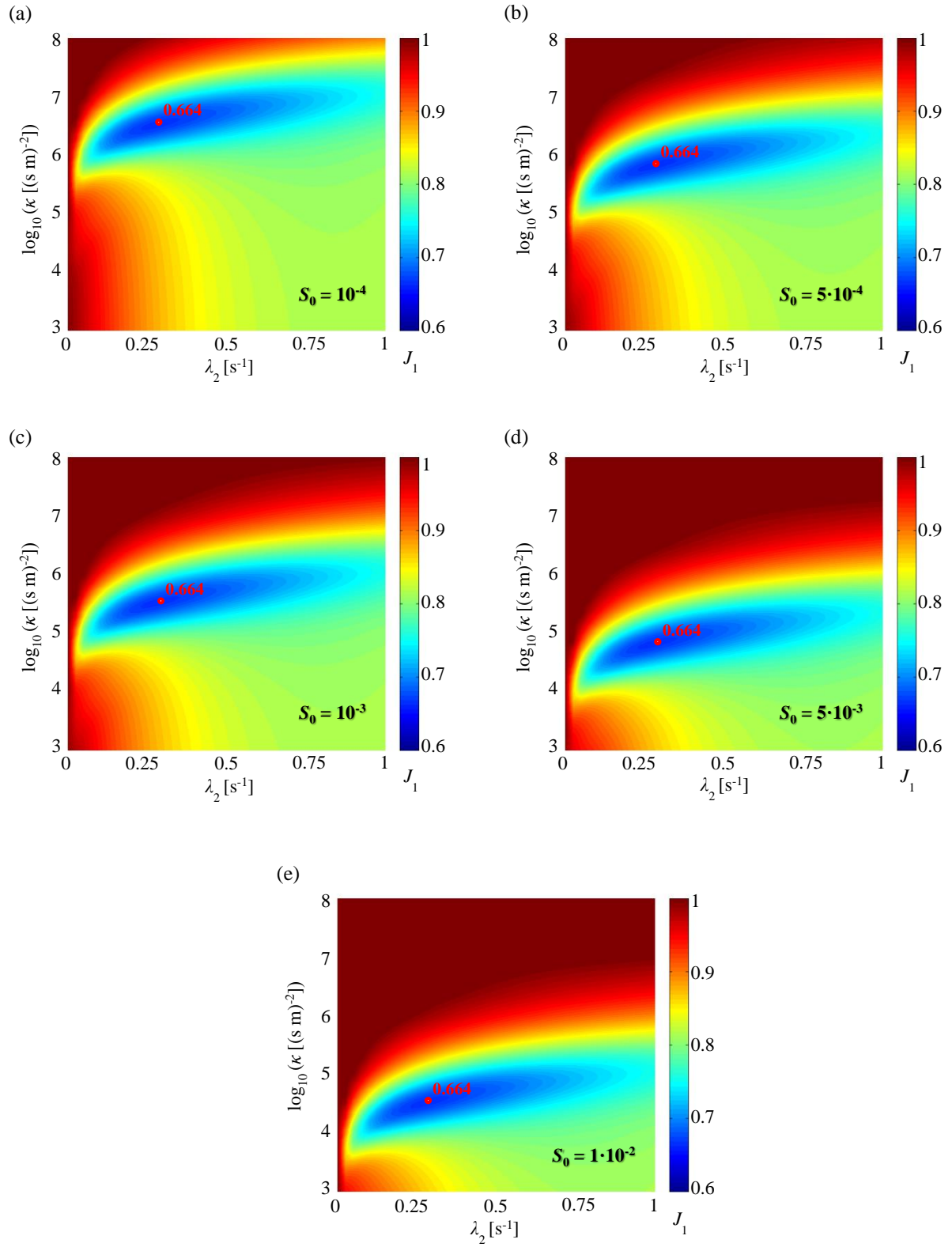
Figure 5: J_1 function with respect to the normalised nonlinear stiffness κ and linear damping λ_2 varying S_0 [(m/s²)²/(rad/s)].

(a)

(b)
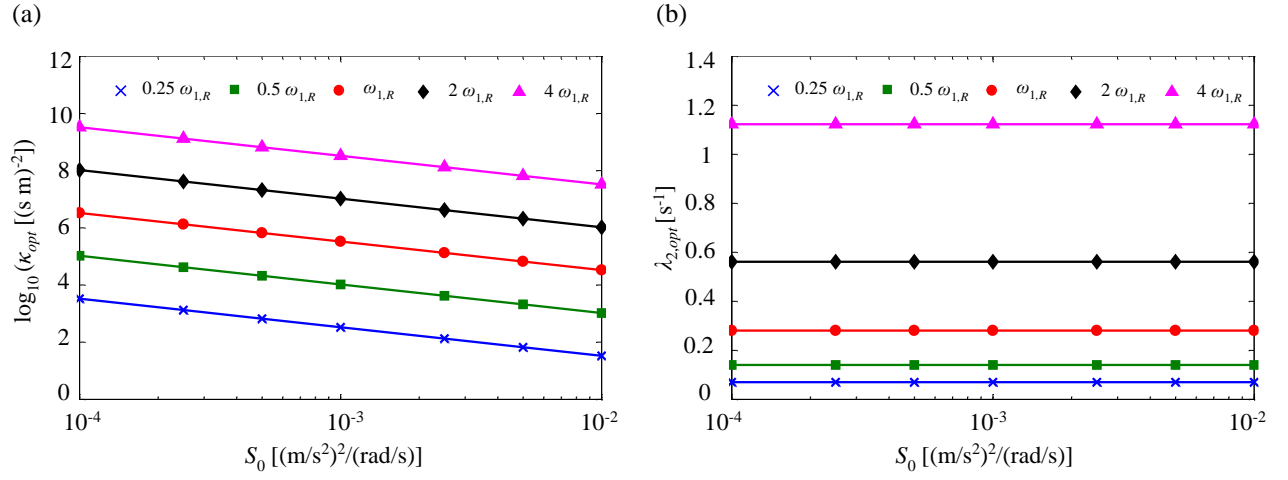
Figure 6: Optimal parameters of the NES obtained by MCS (symbols) and fitted curves (solid line) versus S_0 varying the main frequency ω_1 ($\zeta_1 = \zeta_{1,R}$, $\varepsilon = 0.05$): a) normalised optimal NES stiffness κ; b) normalised optimal NES damping λ_2.

(a)

(b)
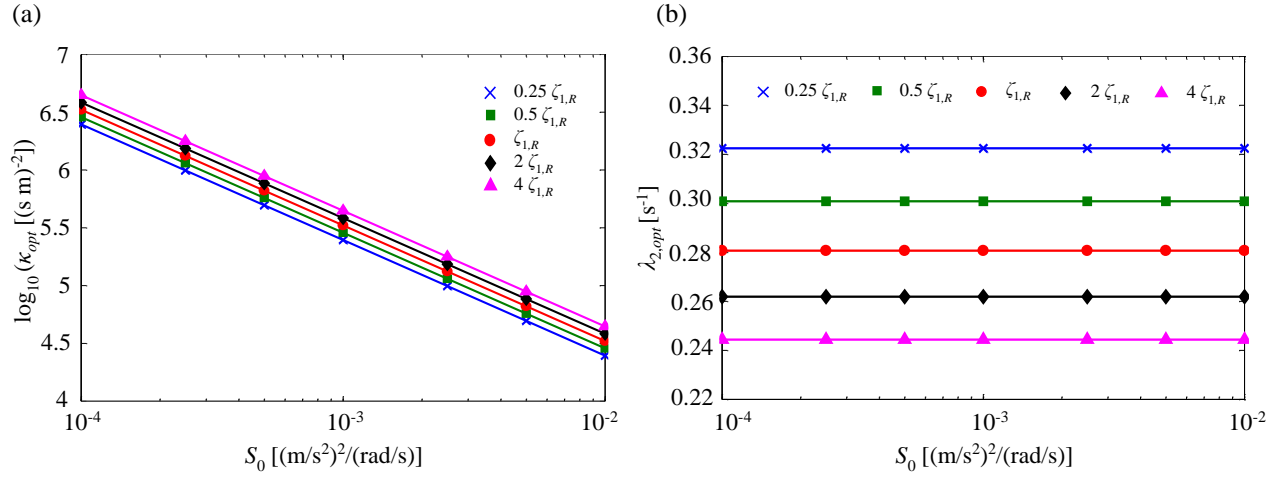
Figure 7: Optimal parameters of the NES obtained by MCS (symbols) and fitted curves (solid line) versus S_0 varying the main damping ratio ζ_1 ($\omega_1 = \omega_{1,R}$, $\varepsilon = 0.05$): a) normalised optimal NES stiffness κ; b) normalised optimal NES damping λ_2.

(a)

(b)
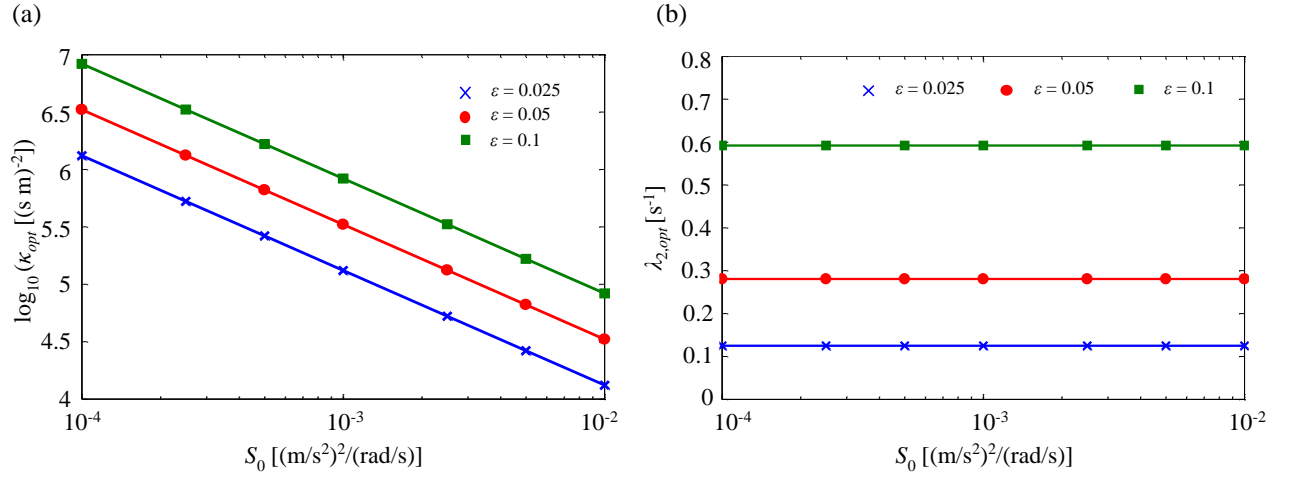
Figure 8: Optimal parameters of the NES obtained by MCS (symbols) and fitted curves (solid line) versus S_0 varying the mass ratio ε ($\omega_1 = \omega_{1,R}$, $\zeta_1 = \zeta_{1,R}$): a) normalised optimal NES stiffness κ; b) normalised optimal NES damping λ_2.
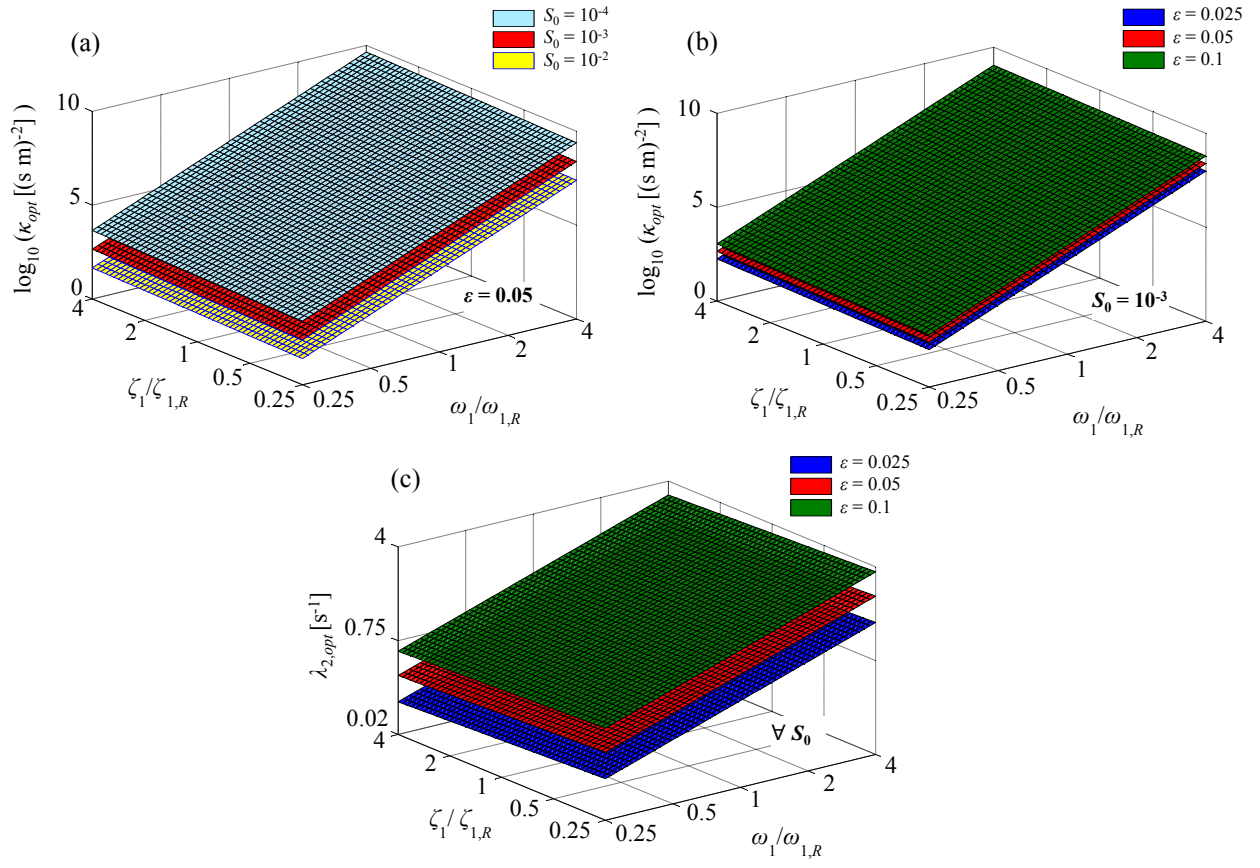
Figure 9: Optimal NES parameters for varying normalised frequency and damping of the primary structure: a) κ_{opt} for fixed ε; b) κ_{opt} for fixed S_0; c) $\lambda_{2,opt}$.
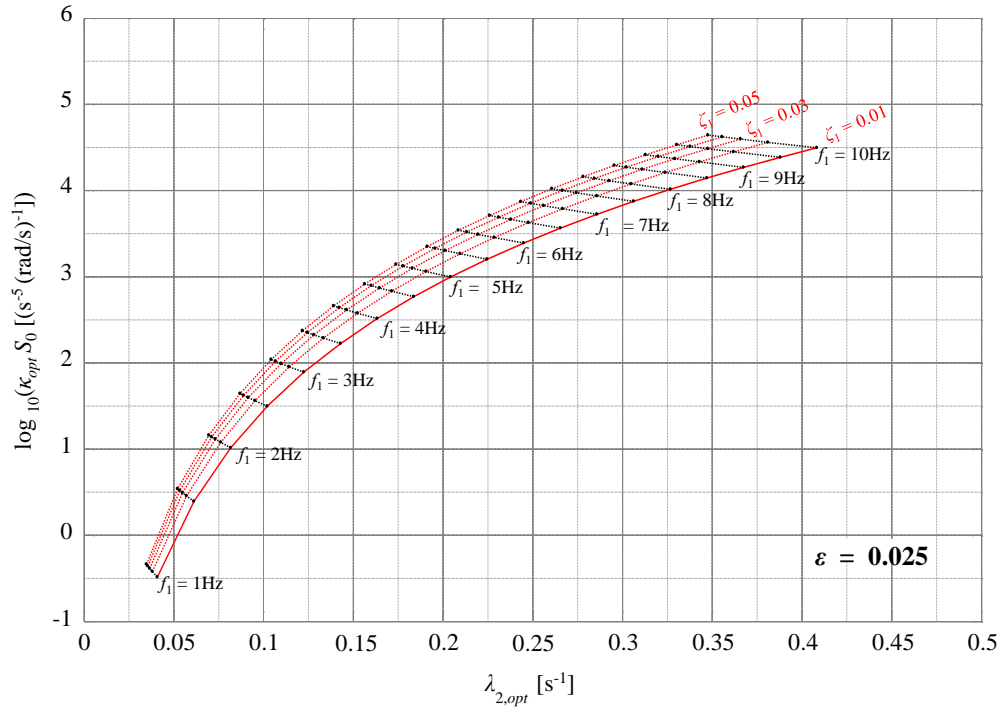
Figure 10: Design chart to determine the optimal NES parameters for different values of ω_1 and ζ_1 ($\varepsilon = 0.025$).
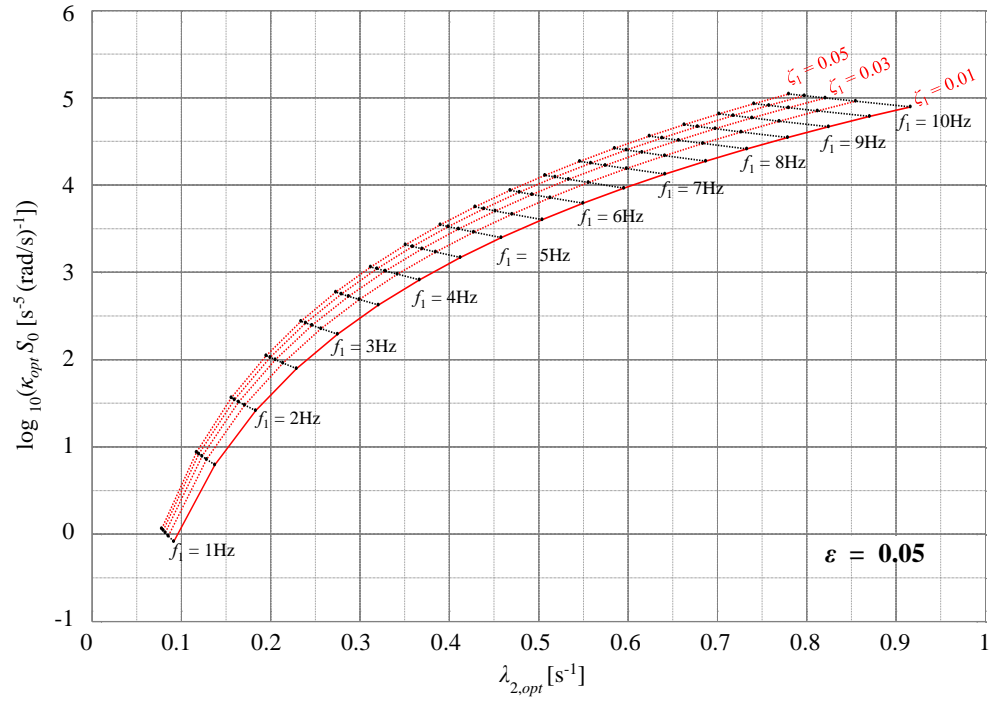
Figure 11: Design chart to determine the optimal NES parameters for different values of ω_1 and ζ_1 ($\varepsilon = 0.05$).
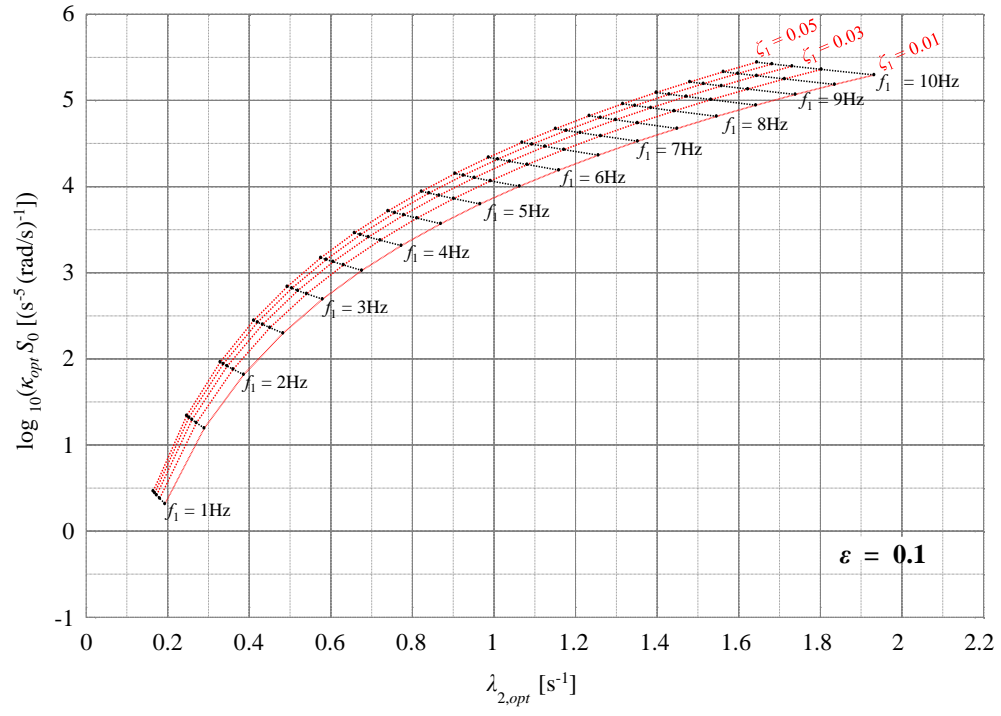
Figure 12: Design chart to determine the optimal NES parameters for different values of ω_1 and ζ_1 ($\varepsilon = 0.1$).
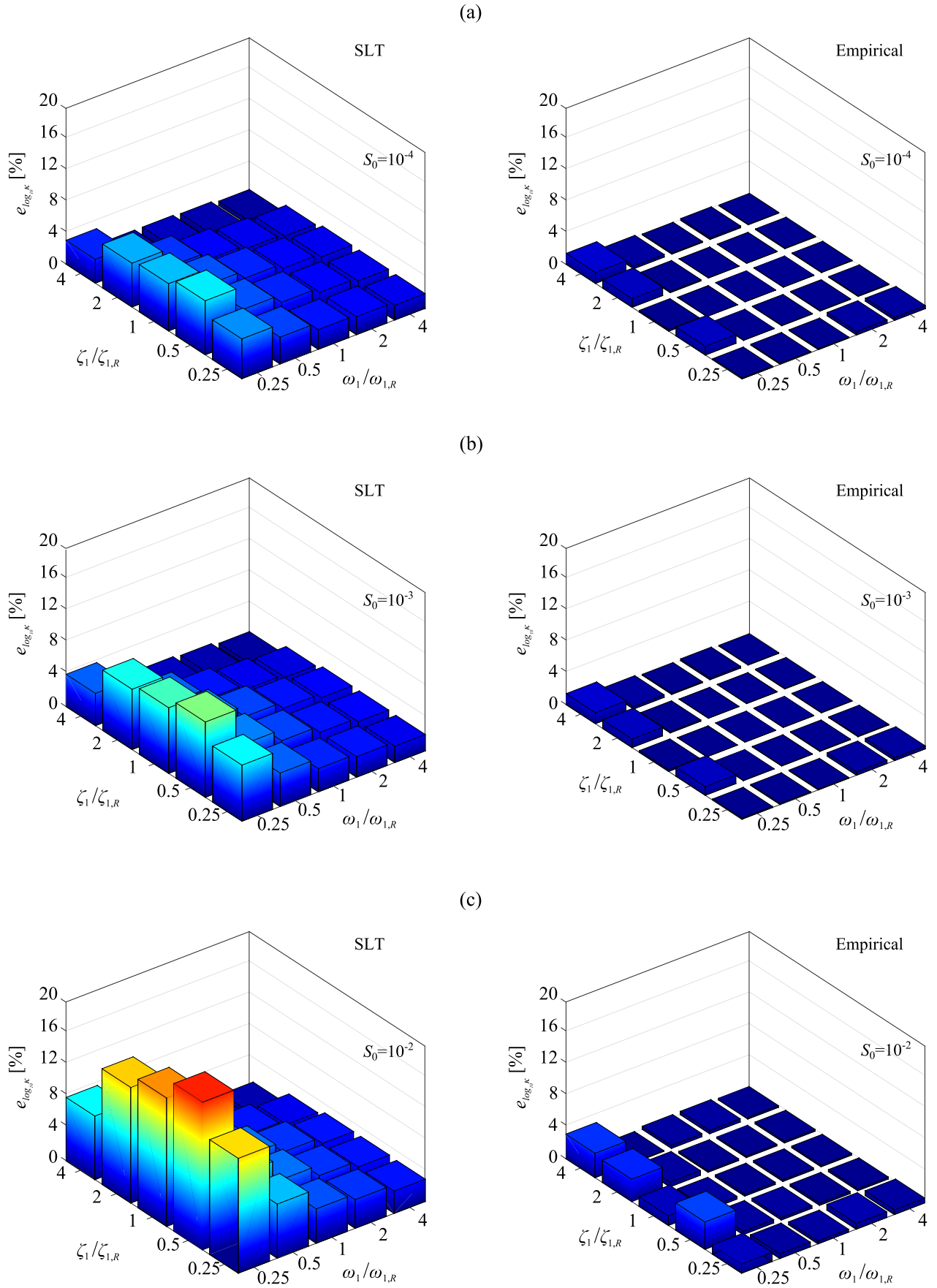
Figure 13: Percentage error commited in the evaluation of the NES optimal stiffness in logarithmic scale by using the SLT-based formula (20) and the empirical formula (28) for ε = 0.05 and : a) $S_0 = 10^{-4}$ (m/s²)²/(rad/s); b) $S_0 = 10^{-3}$ (m/s²)²/(rad/s); c) $S_0 = 10^{-2}$ (m/s²)²/(rad/s).
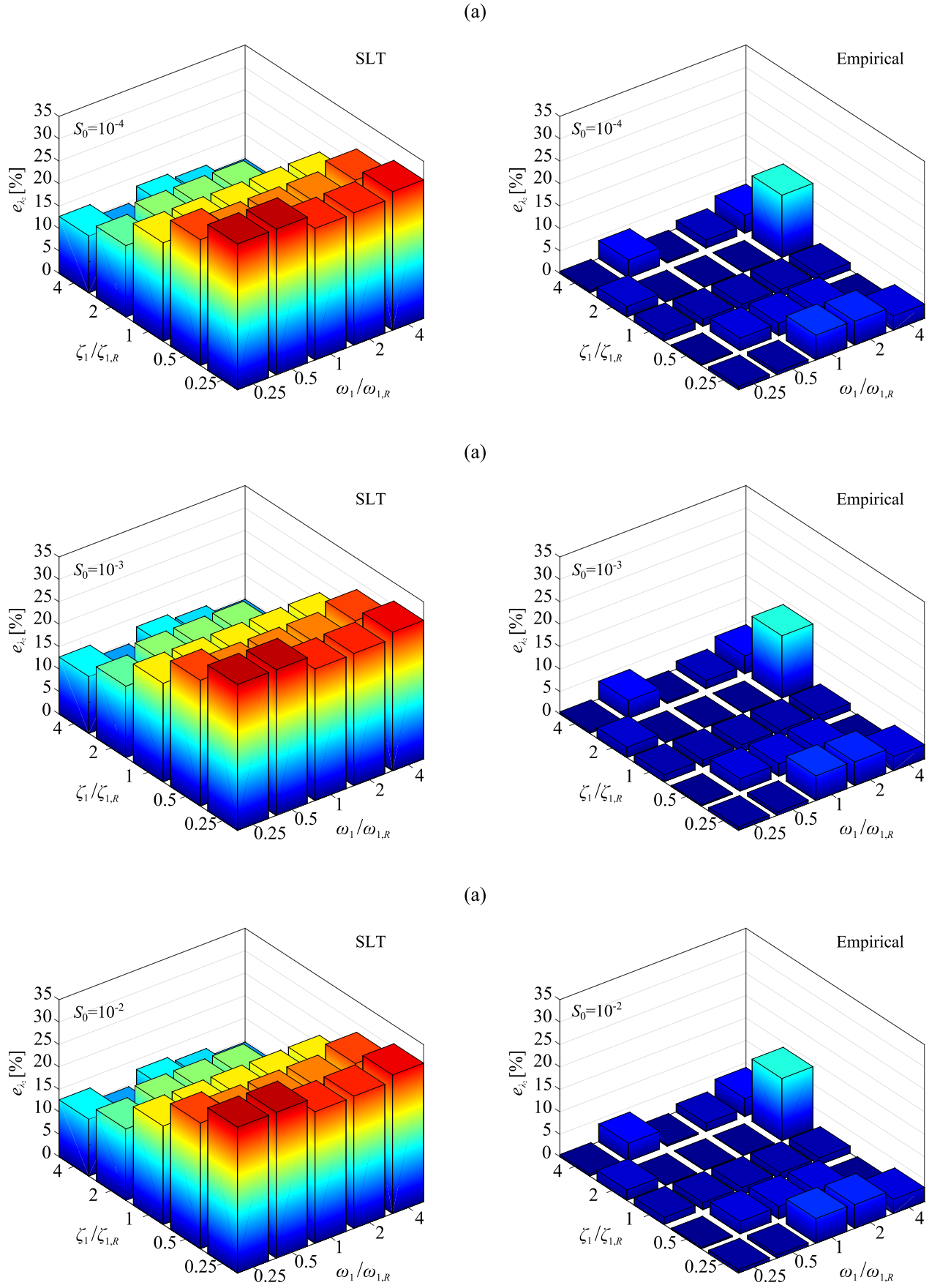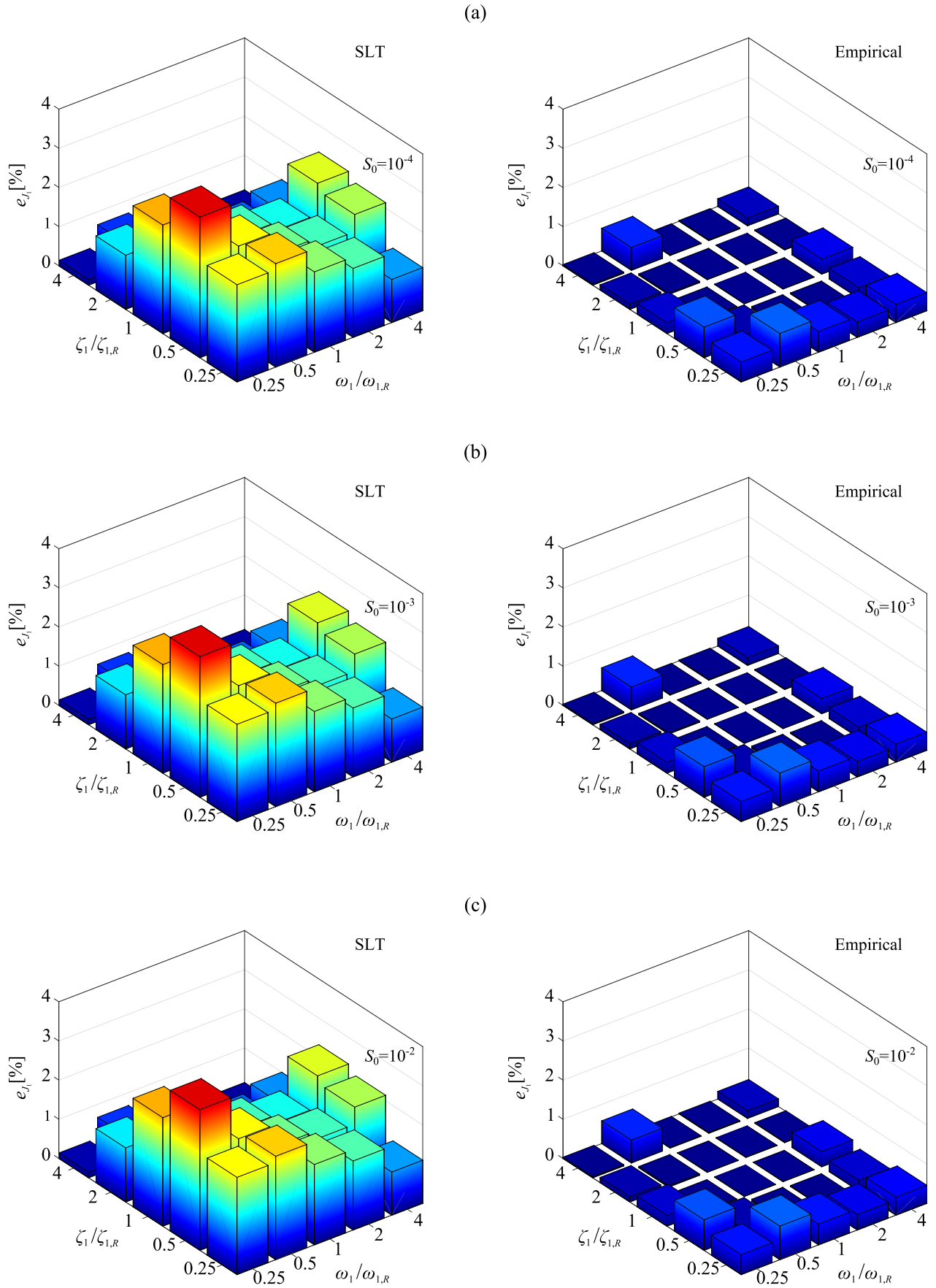
Figure 14: Percentage error commited in the evaluation of the NES optimal damping by using the SLT-based formula (21) and the empirical formula (29) for $\varepsilon = 0.05$ and: a) $S_0 = 10^{-4}$ $(m/s^2)^2/(rad/s)$; b) $S_0 = 10^{-3}$ $(m/s^2)^2/(rad/s)$; c) $S_0 = 10^{-2}$ $(m/s^2)^2/(rad/s)$.

Figure 15: Percentage error commited on the estimation of the minimum of the J_1 function by using the SLT-based approach and the empirical approach for $\varepsilon = 0.05$ and: a) $S_0 = 10^{-4}$ $(m/s^2)^2/(rad/s)$; b) $S_0 = 10^{-3}$ $(m/s^2)^2/(rad/s)$; c) $S_0 = 10^{-2}$ $(m/s^2)^2/(rad/s)$.
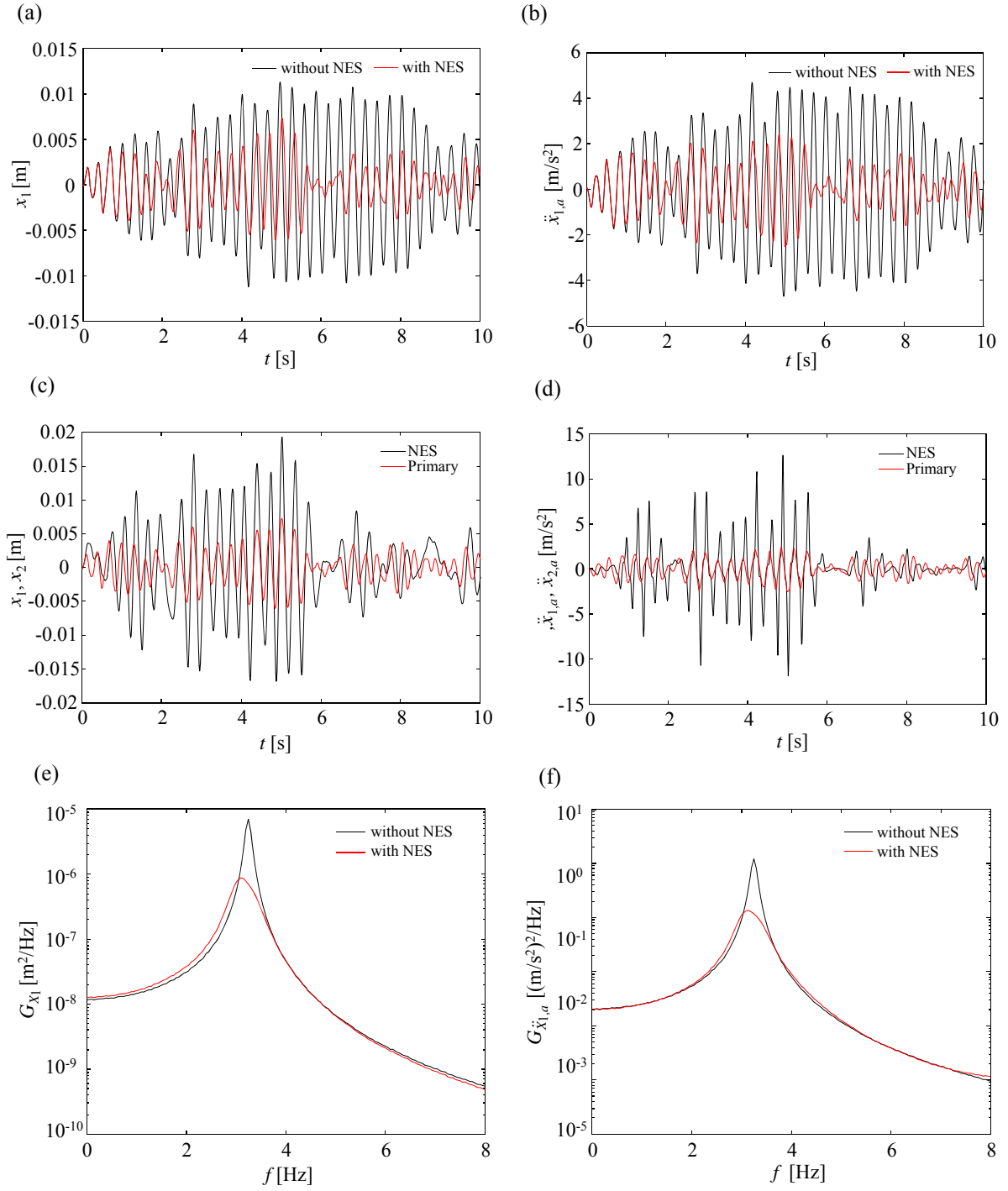
Figure 16: Comparison between the uncontrolled and controlled configurations in time and frequency domain: a) first 10 sec of a sample of structural displacements process; b) first 10 sec of a sample structural accelerations process; c) first 10 sec of a sample of displacements process of the NES and primary structure; d) first 10 sec of a sample of accelerations process of the NES and primary structure; e) PSD of displacements process; f) PSD of absolute accelerations process.
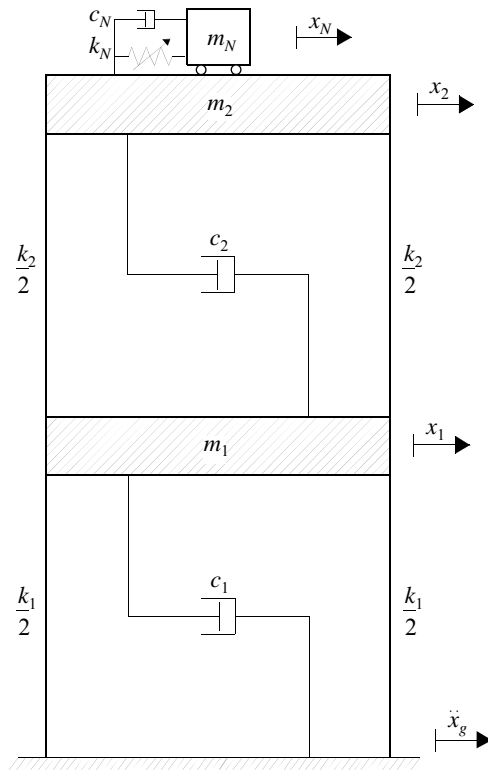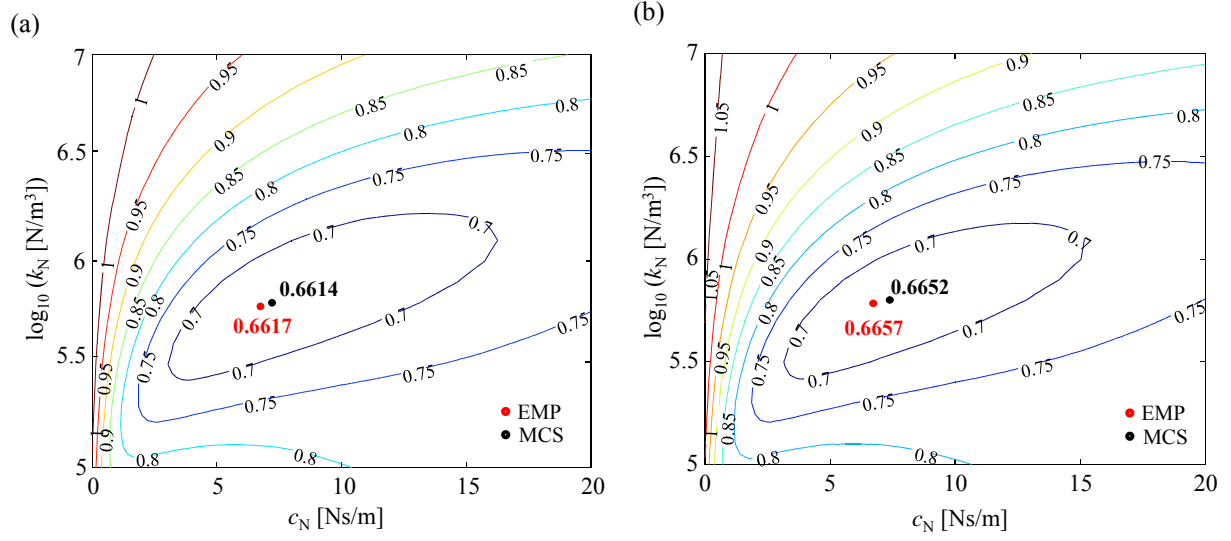
Figure 17: 2-DOF structure coupled with a NES.

Figure 18: Objective functions and optimal NES parameters obtained by MCS (black dots) and by using the empirical formulae (red dots): a) J_1; b) J_2.
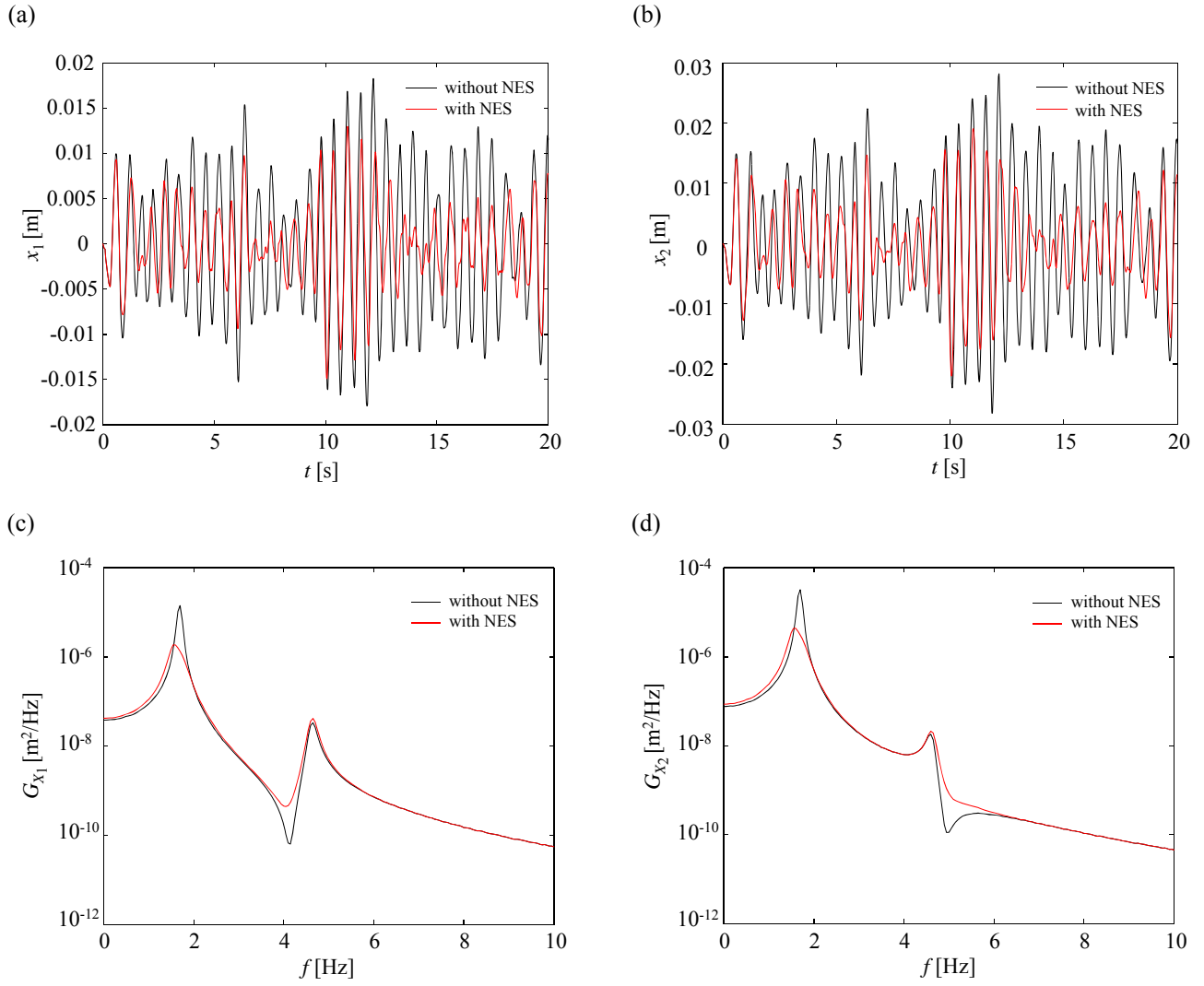
Figure 19: Comparison between the uncontrolled and controlled configurations in time and frequency domain: a) a sample of first storey displacements process; b) a sample of second storey displacements process; c) PSD of first storey displacements; d) PSD of second storey displacements.